

Thesis 997

UNIVERSITY OF STIRLING

TESTS OF QUANTUM MECHANICS VERSUS LOCAL REALISM
USING AN ATOMIC DEUTERIUM SOURCE

TORLA BIN HAJI-HASSAN

B.Sc. (1981), M.Sc. (1984)

Submitted for the Degree of Doctor of Philosophy

Atomic Physics Laboratory, University of Stirling,

FK9 4LA, United Kingdom.

December 1987

ABSTRACT

Measurements of the polarization correlation of the two-photons emitted simultaneously by metastable atomic deuterium in a true second order radiative process, are described. Two experiments, one involving the use of a half-wave plate and two linear polarizers, and the other three linear polarizers, have been carried out to investigate the validity of quantum mechanics in hitherto unexplored situations and to test local realistic theories of the type recently proposed by Garuccio and Selleri. The results of the experiments provide clear evidence against local realistic theories in which the probability of detection is postulated to be dependent on the angle between a polarization vector \vec{I} , and a detection vector $\vec{\lambda}$. The quantum mechanical predictions for such experiments, in which non-ideal analysers were employed, have also been established and have been shown to be in agreement with the experimental results. In addition, the results of circular polarization measurements confirm the conservation of angular momentum along the common axis of detection and give further verification of the correctness of the form of the state vector describing the state of polarization of the two-photons. In another experiment, the effect of an electric field on the polarization properties of the two-photons has been measured for the first time. The Stoke's

parameters characterizing the two-photon beam have been determined and the results suggest that the two-photon radiation is partially polarized at 22.5° with respect to the electric field vector. It is suggested that the effect is due to the removal of the degeneracy of the virtual intermediate P states of the deuterium atom.

ACKNOWLEDGMENTS

The author would like to gratefully acknowledge his supervisors Professor H. Kleinpoppen and Dr. A. J. Duncan for their invaluable guidance and active involvement at all stages; Professor E. Merzbacher, from the University of North Carolina, Chapel Hill, U.S.A., for the many hours of his time he made available for the discussion of quantum mechanical aspects of the problem; Dr. W. Perrie for his advice and assistance in the laboratory during the first stage of this work and Dr. H. J. Beyer for many helpful discussions.

In addition, the author wishes to express his appreciation to Mr. A. J. Duncan, Mr. A. Sherman and Mr. J. Weir for their technical assistance and the staff of Shared Technical Services for their cooperation.

Finally, the provision of a scholarship by the Government of Malaysia and the International Islamic University, Malaysia during the tenure of which this investigation was undertaken is acknowledged.

CONTENTS

	Page
<u>ABSTRACT</u>	11
<u>ACKNOWLEDGMENT</u>	iv
<u>ILLUSTRATIONS</u>	x
<u>CHAPTER ONE : INTRODUCTION</u>	1
§ 1.1 QUANTUM QUESTIONS AND DEVELOPMENT OF ALTERNATIVE THEORIES	4
1.1.1 <i>The Einstein Podolsky Rosen arguments versus the Copenhagen interpretation of quantum mechanics</i>	4
1.1.2 <i>Development of hidden variable theories and the discovery of Bell's theorem</i>	11
§ 1.2 A BRIEF SURVEY OF PREVIOUS EXPERIMENTAL WORK	18
§ 1.3 THE NO-ENHANCEMENT HYPOTHESIS	23
1.3.1 <i>Local realistic models</i>	24
1.3.2 <i>Proposed experimental tests</i>	25
§ 1.4 PLAN OF THE PRESENT WORK	28

	CHAPTER TWO : THEORETICAL ASPECTS	29
§ 2.1	THE STATE VECTOR AND DENSITY MATRIX REPRESENTATIONS OF THE POLARIZATION STATE OF TWO-PHOTONS	30
2.1.1	<i>Two-photon decay of metastable atomic hydrogen</i>	30
2.1.2	<i>State vector representation of the two-photon pairs</i>	36
2.1.3	<i>Density matrix representation of the two-photon pairs</i>	40
§ 2.2	QUANTUM MECHANICAL REPRESENTATION OF ANALYSERS	43
2.2.1	<i>Normal devices</i>	43
2.2.2	<i>Linear polarizers</i>	45
2.2.3	<i>Two linear polarizers placed in series</i>	46
2.2.4	<i>Retarder</i>	50
2.2.5	<i>Circular polarizers</i>	50
§ 2.3	QUANTUM MECHANICAL PREDICTIONS	53
2.3.1	<i>Polarization correlation analysed by two linear polarizers and a half-wave plate</i>	53
2.3.2	<i>Polarization correlation analysed by three linear polarizers</i>	57
2.3.3	<i>Circular polarization analysis</i>	60

	CHAPTER THREE : EXPERIMENTAL WORK	63
§ 3.1	APPARATUS	64
3.1.1	<i>The production of the metastable</i>	
	<i>atomic beam</i>	66
	a) <i>Ion source</i>	67
	b) <i>Cesium cell</i>	67
	c) <i>Electric field plates</i>	68
3.1.2	<i>Optical systems</i>	68
	a) <i>Pile-of-plates polarizers</i>	69
	b) <i>Retarders</i>	69
3.1.3	<i>Vacuum system</i>	70
3.1.4	<i>Lyman alpha detection system</i>	70
3.1.5	<i>Data acquisition system</i>	71
3.1.6	<i>System Interlock</i>	72
§ 3.2	EXPERIMENTAL TECHNIQUES	74
3.2.1	<i>The production of the metastable</i>	
	<i>atomic deuterium beam</i>	74
3.2.2	<i>Determination of the optical parameters</i>	75
	a) <i>The transmittances of</i>	
	<i>imperfect polarizers</i>	75
	b) <i>Determination of the</i>	
	<i>interference factor</i>	80
3.2.3	<i>Optimum conditions</i>	81
	a) <i>Optimization of signal to</i>	
	<i>noise ratio</i>	81
	b) <i>Focussing condition</i>	84

3.2.4	<i>The method of gathering data</i>	84
	a) <i>Normalization procedure</i>	84
	b) <i>Background coincidence rate</i>	85
	CHAPTER FOUR : RESULTS	89
§ 4.1	TWO LINEAR POLARIZERS AND A HALF-WAVE PLATE	88
	i) <i>Measurements</i>	88
	ii) <i>Results</i>	90
	iii) <i>Comparison of the results with the predictions of quantum mechanics and local realism</i>	93
§ 4.2	THREE LINEAR POLARIZERS	96
	i) <i>Measurements</i>	96
	ii) <i>Results</i>	97
	iii) <i>Comparison of the results with the predictions of quantum mechanics and local realism</i>	102
§ 4.3	CIRCULAR POLARIZERS	103
	i) <i>Measurements</i>	103
	ii) <i>Results</i>	104
	iii) <i>Comparison of the results with the predictions of quantum mechanics and local realism</i>	106

§ 4.4	THE EFFECTS OF AN ELECTRIC FIELD	108
	<u>CHAPTER FIVE : CONCLUSION</u>	112
	<u>REFERENCES</u>	117
	<u>APPENDIX :</u>	
	<u>DESCRIPTIONS OF THE POLARIZATION OF LIGHT</u> ..	123
§ A.1	QUANTUM MECHANICAL DESCRIPTION OF PHOTONS ..	124
A.1.1	<i>State vector</i>	124
A.1.2	<i>Photon state vector in linear and</i> <i>circular polarization bases</i>	127
A.1.3	<i>Density matrix</i>	128
§ A.2	CLASSICAL DESCRIPTION OF THE POLARIZATION OF LIGHT	134

ILLUSTRATIONS

	Page
Figure 1.1. The most common experimental arrangement used for two photon polarization correlation measurements. D1 and D2 are photomultipliers	16
Figure 1.2. Comparison of local realistic and quantum mechanical predictions for ideal experiments	16
Figure 2.1. Theoretically predicted two-photon spectral distribution for metastable hydrogen	32
Figure 2.2. Feynman diagrams representing the spontaneous simultaneous emission of two-photons	35
Figure 2.3. Energy level diagram of the first two levels of atomic hydrogen neglecting hyperfine structure (not to scale). The two photons frequencies ν_1 and ν_2 can have any energy provided $h\nu_1 + h\nu_2 =$	

10.2 eV. The important decay
modes are shown - - - - - 37

Figure 2.4. The orientation of the linear
polarizers with respect to
the x-axis - - - - - 57

Figure 3.1. Schematic diagram of the
apparatus - - - - - 65

Figure 3.2. Schematic diagram of the
detection system - - - - - 73

Figure 3.3. The transmittance of polarizer B
as a function of θ , where θ is
the angle between the
transmission axis of polarizer B
and the x-direction - - - - - 78

Figure 3.4. The transmittance of polarizer A
as a function of θ , where θ is
the angle between the
transmission axis of polarizer A
and the x-direction - - - - - 78

Figure 3.5. The transmittance of polarizer C
as a function of θ , where θ is

the angle between the
transmission axis of polarizer C
and the x-direction - - - - - 79

Figure 3.6. The variation of the intensity as
a function of the angle α while
the angle β was fixed at 33° and
 67.5° - - - - - 82

Figure 3.7. The three dimensional plots of
the variation of the normalized
intensity as a function of the
angles α and β - - - - - 83

Figure 3.8. A typical coincidence spectrum.
Total collection time is 165 hours.
The peak FWHM = 27 channels,
equivalent to 3 ns, approximately
equal to the timing resolution of
the electronic detection system - - - - - 86

Figure 4.1. Schematic diagram of the $\lambda/2$ -wave
plate and two polarizer
experiment - - - - - 89

Figure 4.2. The variation of the normalized
coincidence signal $R(\theta)/R(\infty)$,

where $R(\theta)$ is the coincidence rate as a function of θ , the angle between the transmission axis of polarizer B and the x-direction. The fast axis of the $\lambda/2$ -wave plate was rotated through angle $\theta/2$. The quantity $R(\infty)$ is the coincidence rate obtained with the half-wave plate in place and the plates of both linear polarizers removed. The solid curve represents the quantum mechanical prediction ... 91

Figure 4.3. The variation of the normalized coincidence signal $R(\theta)/R(\infty)$ as the fast axis of the $\lambda/2$ -wave plate was rotated through angle θ ... 92

Figure 4.4. A plot of the singles rate as the fast axis of the $\lambda/2$ -wave plate was rotated through angle θ ... 92

Figure 4.5. Coincidence signal as a function of the angle θ between the transmission axes of the

polarizers, relative to $R(\theta)$, the coincidence signal with the polarizer plates removed. The solid curve represents the quantum mechanical prediction (Perrie et al[27]) - - - - - 95

Figure 4.6. Schematic diagram of the three polarizer experiment - - - - - 96

Figure 4.7. Variation of the ratio $R(\beta, \alpha)/R(\beta, \theta)$, for $\beta = 0^\circ$ and 33° , as a function of α . The quantum mechanical prediction for $\beta = 0^\circ$ is shown as the solid curve whereas the upper limit for various angles β set by theories of the Garuccio - Selleri type is shown as a dotted line - - - - - 98

Figure 4.8. Variation of the ratio $R(\beta, \alpha)/R(\beta, \theta)$ as a function of α , for $\beta = 0^\circ, 33^\circ$ and 67.5° . The solid curves represent the quantum mechanical predictions - - - - - 99

Figure 4.9. Variation of the ratio $R(\beta, \alpha)/R(\beta, \infty)$ as a function of α , for $\beta = \pm 45^\circ$. The solid curves represent the quantum mechanical predictions - - - - - 100

Figure 4.10. Schematic diagram of the circular polarizer experiment - - - - - 103

Figure 4.11. Coincidence signal $R(\alpha)$ (α is the angle between the fast axis of the $\lambda/4$ -wave plate and the x-axis) relative to $R(\infty)$ (the coincidence signal with the polarizer plates removed). The solid curves represent the quantum mechanical predictions - - - - - 105

Figure 4.12. Normalized coincidence signal of the two-photons in the presence of an electric field ($E = 30 \text{ V cm}^{-1}$) as a function of θ , the angle between the transmission axis of polarizer B and the electric field vector (x-axis). Quantum mechanical prediction for $E = 0 \text{ Vcm}^{-1}$ is shown as a solid curve - - - - - 109

CHAPTER ONE
INTRODUCTION

Up to the end of the nineteenth century, physicists had a comprehensive notion of the way the universe works. The general philosophical view held by physicists was that of deterministic mechanism. However, the triumph of classical physics was short-lived since it failed to explain atomic phenomena and in 1925, Heisenberg with the help of Born, Pauli and Jordan pioneered the world's first quantum theory, called matrix mechanics. Subsequently, in the same year, Schrödinger and Dirac independently developed, along different lines, two additional quantum mechanical theories. These formalisms were quickly proved to be equivalent to each other and to the matrix mechanics of Heisenberg. Quantum theory represents one of the most remarkable intellectual achievements of the twentieth century. It has been and continues to be overwhelmingly successful in explaining a vast range of physical phenomena at all levels reached by modern experimental physics. There appears to be no real evidence, to date, pointing to its possible limitations, so that already, in 1929, Dirac[1] could write "The underlying physical laws necessary for the mathematical theory of a large part of physics and the whole of chemistry are thus completely known

However, the advent of this theory has created a confusion as to what sort of reality, if any, lies behind the everyday world and an unprecedented controversy as to

what the theory actually means because of its indeterminism and non-locality. Einstein, particularly, found this lack of determinism in a physical theory undesirable and summed up his feelings in the oft quoted phrase "God does not play dice". Bohr, who accepted quantum ideas completely, is reported to have replied "Don't tell God what to do!". Einstein also indicated his unhappiness with non-locality of quantum mechanics in the well known phrase "Spooky actions at a distance". Other eminent physicists who contributed to the development of quantum mechanics, e.g. Planck, Schrödinger and de Broglie, expressed deep concern over its final formulation.

In this chapter, we shall present, in the first section, an overall view to this controversial subject. We then review in the second section the experimental evidence for and against quantum theory. The penultimate section is devoted to a discussion of the concepts motivating the present experimental work which itself is described in the last section.

§ 1.1 QUANTUM QUESTIONS AND DEVELOPMENT OF ALTERNATIVE THEORIES

1.1.1 The Einstein - Podolsky - Rosen Arguments Versus the Copenhagen Interpretation of Quantum Mechanics

The paradoxes of quantum theory have occupied the minds of eminent physicists as well as philosophers for decades. The theory is indeterministic since, although the time evolution of the wavefunction Ψ is strictly determined by the Schrödinger equation, the quantity $|\Psi|^2$ is interpreted as a probability density which only allows predictions to be made in a statistical sense. Thus, the behaviour of an individual member of an ensemble of systems must be considered to be acausal. The central idea of the standard interpretation of quantum mechanics, known as the Copenhagen Göttingen interpretation by Bohr[2], is that a quantity (e.g. momentum) can be considered real only if it has been measured or if the outcome of an experiment to measure the quantity is predictable. This interpretation, advocated by Heisenberg and Born, clearly requires a radical departure from classical notions regarding the nature of measurement and is in direct conflict with at least one of the following three premises which most people would consider natural and obvious:

- 1) *Realism.* The existence and nature of the universe, considered to be made up of separable entities, are independent of observers. Human consciousness does not play any role in determining the attributes of the entities making up the universe.
- 2) *Causality.* Causal influence propagates always forward in time. Such influence can be defined as the necessary relationship between objects, events, conditions or other things at a given time and those at later times. Quantum mechanically, no causal description can be given as to why a particular eigenvalue results in a given measurement. The wavefunction Ψ is used merely as a tool for making prediction of the relative probability for the different outcomes when the given quantum system interacts with the measurement apparatus.
- 3) *Locality or separability.* Regarding locality, it is the requirement that no signal nor influence of any kind can propagate faster than the speed of light. Hence, if A and B are two space-time points separated from each other by a space-like interval, then the results of measurements made at B cannot influence the results of measurements made at A and vice versa. This definition corresponds to what is often referred to as Einstein locality. On the other hand, in quantum mechanics, if two system have interacted in the past it is, in general, not possible after the interaction

to assign a single state vector to either of the two systems. This statement amounts to what is called the principle of non-separability.

These three assumptions form the basis of the so-called local realistic theories. The incompatibility of quantum theory with these intuitive principles is the issue raised by the celebrated *Einstein Podolsky Rosen (EPR) paradox*(3). In the paper, published in 1935, entitled 'Can Quantum Mechanical Description of Physical Reality be Considered Complete?', Einstein, Podolsky and Rosen proposed a thought experiment and analysed the implications of the predictions of quantum mechanics for the outcome of the experiment. The philosophical realist requirement put forward by Einstein, Podolsky and Rosen as a necessary condition for a complete theory was that: "Every element of the physical reality must have a counterpart in the physical theory". They also introduced the concept of *an element of physical reality* through the criterion: "If without in any way disturbing a system, we can predict with certainty (i. e. with probability equal to unity) the value of a physical quantity (the value of an observable), then there exists an element of physical reality corresponding to this physical quantity". By considering a system of two spatially separated but quantum mechanically correlated particles which had previously interacted, they showed that two physical

quantities described by non-commuting operators could have simultaneous reality, contrary to the quantum mechanical description. It was, therefore, concluded by Einstein, Podolsky and Rosen that quantum mechanics is *incomplete* since there exist elements of physical reality which have *no counterpart in the physical theory*.

In order to illustrate their ideas, Einstein, Podolsky and Rosen considered a system consisting of two particles, 1 and 2, described by the position variables x_1 and x_2 . After some interaction, the composite system could be represented by the wavefunction

$$\Psi(x_1, x_2) = \int_{-\infty}^{\infty} \exp \left[\frac{i2\pi(x_1 - x_2 + x_0)p}{h} \right] dp, \quad (1.1)$$

where x_0 is an arbitrary constant. The wavefunction above can be rearranged to give

$$\Psi(x_1, x_2) = \int_{-\infty}^{\infty} \exp \left[\frac{-i2\pi(x_2 - x_0)p}{h} \right] \exp \left[\frac{i2\pi x_1 p}{h} \right] dp, \quad (1.2)$$

where $\exp(i2\pi x_1 p/h)$ is the eigenfunction of the linear momentum operator $(h/2\pi i)\partial/\partial x_1$, corresponding to the value p for momentum of particle 1, whereas $\exp[-i2\pi(x_2 - x_0)p/h]$ is the eigenfunction of the linear momentum operator $(h/2\pi i)\partial/\partial x_2$ corresponding to the value $-p$ for momentum of particle 2. Now supposing that the result of a momentum measurement on particle 1 is found to have the

value p then, we can predict with certainty, without in any way disturbing particle 2, that a momentum measurement on particle 2 will yield the value $-p$. Hence, in the context of the EPR argument, the momentum of particle 2 with value $-p$ is *an element of reality*. However, one can also write the wavefunction in the form

$$\begin{aligned}\Psi(x_1, x_2) &= \int_{-\infty}^{\infty} \left\{ \int_{-\infty}^{\infty} \exp i \frac{[2\pi i(x_1 - x_2 + x_0)p]}{h} dp \right\} \delta(x_1 - x) dx \\ &= h \int_{-\infty}^{\infty} \delta(x_1 - x_2 + x_0) \delta(x_1 - x) dx, \\ &\dots\dots\dots (1.3)\end{aligned}$$

where $\delta(x, -x)$ is the eigenfunction of the position operator x_1 corresponding to the coordinate x for particle 1 and, similarly, $\delta(x, -x_2 + x_0)$ is the eigenfunction of the position operator x_2 corresponding to the coordinate $x + x_0$ for particle 2. Supposing that the result of a measurement on particle 1 is found at a position with coordinate x then, we can predict with certainty, without in any way disturbing particle 2, that a position measurement on particle 2 will yield the value $x + x_0$ and hence, on the basis of the EPR criterion of physical reality, we can say that *an element of reality* corresponds to the position coordinate of particle 2 with value $x + x_0$. Consequently, the values of momentum and position pertaining to particle 2 are two elements of

physical reality, regardless of whether the measurements on particle 2 are performed or not. However, according to the doctrine of quantum mechanics, the position and the momentum of particle 2 cannot have simultaneously precise values since x_2 and $(h/2\pi i)\partial/\partial x_2$ are non-commuting operators. These arguments lead to the conclusion, as before, that the quantum mechanical description is not a complete description of physical reality. In order that the theory be complete in the sense defined by them, Einstein, Podolsky and Rosen further suggested the necessity for the introduction of hidden variables, which, it was hoped, at one and the same time, would restore determinism to physics and explain in a rational way the nonlocality implied by the principle of non-separability.

However, Bohr(4), the principal protagonist in the epic debate on this subject rejected the conclusion of Einstein, Podolsky and Rosen, and challenged their argument regarding the meaning of "physical reality". He summarized his position as follows: "From our point of view we now see that the wording of the above-mentioned criterion of physical reality proposed by Einstein, Podolsky and Rosen contains an ambiguity as regards the meaning of expression *without in any way disturbing a system*" when it is applied to quantum phenomena. In accordance with Bohr's arguments with regard to the EPR

thought experiment, if one makes a measurement of, say, the position of the particle 1, then it would "allow an essentially uncontrollable momentum" to pass from the particle 1 into the measuring device so that we have "cut ourselves off from any future possibility of applying the law of conservation of momentum to the system and therefore have lost our only basis for an unambiguous application of the idea of momentum in predictions regarding the behaviour of the second particle (particle 2)". On the other hand, if we choose to measure the momentum of one of the particles, "we lose through the uncontrollable displacement inevitable in such a measurement any possibility of deducing from the behaviour of this particle the position of the measuring device relative to the rest of the apparatus, and have thus no basis whatever for predictions regarding the location of the other particle". He continued saying: "of course there is in a case like that just considered no question of mechanical disturbance of the system under investigation during the last critical stage of the measuring procedure. But even at this stage there is essentially the question of an influence on the very conditions which define the possible types of predictions regarding the future behaviour of the system. Since these conditions constitute an inherent element of the description of any phenomena to which the term *physical reality* can be properly attached, we see that the

argumentation of the mentioned authors does not justify their conclusion that quantum mechanical description is essentially incomplete". He maintained that measurement on particle 1 does not produce a direct mechanical disturbance on the physical reality pertaining to particle 2, but changes our knowledge about the system. He then pointed out that the whole realistic viewpoint is inapplicable to microscopic systems and the term *physical reality* could not be used to describe an observed object in isolation, but could only be applied meaningfully to the observed object and measuring apparatus together regarded as an *indivisible whole*. He concluded that the quantum mechanical description of physical reality is complete.

1.1.2 Development of Hidden - Variables Theories and the Discovery of Bell's Theorem

A number of theories have been invented in an attempt to provide a viable alternative formulation of quantum mechanics. The theories are called *hidden-variables theories*. Advocates of these theories try to explain the statistical predictions of quantum mechanics by introducing new variables corresponding to underlying deterministic substructures in its equations.

In 1932, von Neumann[5] proposed a theorem which proved the impossibility of a deterministic hidden variables

completion of quantum mechanics. He stated that "we need not go any further into the mechanism of the hidden variable parameters since we now know that the established results of quantum mechanics can never be re-derived with their help". In this way von Neumann effectively stifled further development of hidden-variables theories and greatly supported the acceptance of the Copenhagen interpretation of quantum mechanics. However, in 1951, Bohm[6] developed a hidden variables interpretation of quantum mechanics and claimed that von Neumann's proof was not applicable to this case since the hidden variables were assumed to be dependent on both the state of the observing system and the measuring apparatus. In this theory, hidden variables which are experimentally undetectable, were assumed to be necessary to provide a complete description of a physical reality in addition to a quantum mechanical wavefunction. He also proved that hidden-variables theories were unable to avoid the necessity for non-locality in their formulation if they were to give the same predictions as quantum mechanics. About the same time, in his book, Bohm[7] put forward the argument in terms of a system with discrete, rather than a continuous, distribution of states. He considered a spin-zero system which dissociates into two spin-half systems, where each component of the spin can only take a discrete value. Subsequently, Bohm and Aharonov[8] considered the problem with reference to the

measurements of the polarization correlation of the two γ -ray photons, resulting from the annihilation of para-positronium, carried out by Wu and Shaknov(9). Their experimental results clearly refuted the suggestion made by Schrödinger(10) and Furry(11) that the state vector describing the two-photon pairs might decay spontaneously into a mixture of states, and that, hence, the strength of the correlation of the two-photon pairs might eventually diminish when the photons separated from one another by a distance greater than the coherence length of the wave packets associated with the emitted photons. More recently, a series of more sophisticated experiments has confirmed the observation of Wu and Shaknov.

In 1964, a major discovery took place when Bell(12) carried out an analysis and derived an inequality for a system of two spin-half particles as described by Bohm, after realising that the assumptions of von Neumann were unduly restrictive(13). The now celebrated Bell's inequality exposed in a clear quantitative manner the real nature of the conflict between the predictions of quantum mechanics and those of local realistic theories which exists in the EPR type of experiment. The inequality showed(14) that no realistic theories (stochastic or deterministic hidden-variables theories), satisfying the locality condition, could reproduce all the statistical predictions of quantum mechanics. If the

inequality is violated, then one can explain the experiments only by giving up locality, if realism and a free use of induction are to be retained. Therefore, the world can either be in agreement with quantum theory or it can permit the existence of a local theory; both possibilities are not allowed. The choice lies with experiment.

The original analysis of Bell assumed ideal systems and therefore cannot be tested in a real experimental situation. However, it was then extended by Clauser, Horne, Shimony and Holt (CHSH)[15] and generalized[14] to apply to realisable experiments by assuming that the photons that are not detected have the same properties as those that are detected. This assumption sometimes referred to as the no-enhancement hypothesis, which will be discussed in more detail later (see § 1.3), is made necessary by the low efficiency of photon detectors.

Most experimental work in this field has centred on the measurement of the polarization correlation of the two-photons (in the visible or ultraviolet part of the spectrum) emitted in certain atomic cascades in which an excited atom decays to a lower energy state via an intermediate state with a finite life-time. Figure 1.1 typifies the experimental arrangement. For these experiments, quantum mechanics predicts a stronger correlation between the photon polarization measurements

than local realistic theories, as shown in figure 1.2. Making the no-enhancement hypothesis and assuming that only the relative angle between the transmission axes of the polarizers is significant lead to the Freedman form of Bell's inequality[16], a simple statement of Bell's inequality, involving measurements of only three coincidence rates:

$$\eta \equiv \left| \frac{R(22.5^\circ) - R(67.5^\circ)}{R(\infty)} \right| \leq 0.25 \quad (1.4)$$

where $R(22.5^\circ)$ and $R(67.5^\circ)$ are the coincidence rates when the relative angles between the transmission axes of the polarizers are 22.5° and 67.5° , respectively and $R(\infty)$ is the rate when both polarizers are removed. In the ideal case, represented in figure 1.2, quantum mechanics violates the inequality above, predicting $\eta_{qm} = 0.354$. However, in a real experiment, several factors act to reduce the strength of the quantum mechanically predicted correlations; in certain circumstances to the extent that a violation of the inequality above can no longer be expected to take place. The efficiencies of the polarizers and the finite solid angle of detection are the two main factors which reduce the expected correlation in this way. Local realistic theories generally founder in the light of the results of the

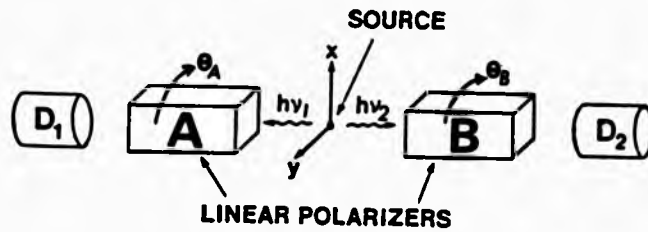


Figure 1.1. The most common experimental arrangement used for two photon polarization correlation measurements. D1 and D2 are photomultipliers.

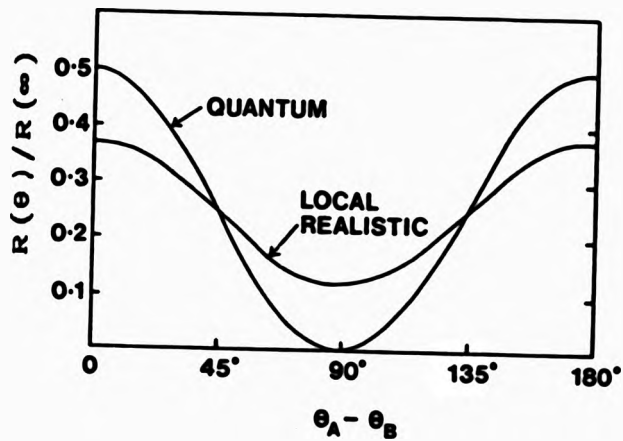


Figure 1.2. Comparison of local realistic and quantum mechanical predictions for ideal experiments.

experiments performed to date (discussed in detail in § 1.2). It is important to note here that,

1) although the photon appears to be influenced by a distant apparatus in all the experiments performed, it is not the kind of influence which can be used to transmit information or signals from one place to another. Therefore, if this influence cannot be used to carry information, then it is *not* in direct conflict with the relativity theory,

and,

2) if the concept of an independent or external reality is to be retained, as a possible explanation of the experimental results, then the quantum mechanical concept of non-separability is a necessary property of that independent reality, albeit a counterintuitive property.

§ 1.2 A BRIEF SURVEY OF PREVIOUS EXPERIMENTAL WORK

In this section we shall review the series of experiments which have been performed recently, using low-energy photons, to test the inequality of the type originally proposed by Bell[12].

1) Freedman and Clauser[17, 18] (1972)

The extension of the proof of Bell to a realizable system by Clauser, Horne, Shimony and Holt led to a first experimental test between the prediction of quantum mechanics and that of local hidden variable theories by Freedman and Clauser. In this experiment the $3d4p^1P_1$ state of calcium in a beam, whose density was $\approx 3 \times 10^{16} \text{ cm}^{-3}$, was excited by radiation from a deuterium arc lamp ($\lambda = 227.5 \text{ nm}$). The polarization correlation was measured for the two photons of wavelengths 551.3 nm and 422.7 nm emitted in $4p^2^1S_0 - 4s4p^1P_1 - 4s^2^1S_0$ cascade in calcium. The two photons were analysed by pile-of-plates polarizers whose transmission efficiencies were $\approx 97\%$. The value of $\eta = 0.300 \pm 0.008$ was obtained in clear violation of the Freedman form of Bell's inequality and in good agreement with the prediction of quantum mechanical theory $\eta_{qm} = 0.301 \pm 0.007$.

ii) Holt and Pipkin[19] (1973)

In this experiment the zero nuclear-spin isotope ^{199}Hg was excited to the 9^1P_1 state by a 100 eV electron beam. The excited atoms decayed via the $9^1\text{P}_1 - 7^3\text{S}_1 - 6^3\text{P}_0$ cascade emitting two photons with wavelengths $\lambda = 567.6$ nm and 404.7 nm. Calcite type polarizers, which possess a much better extinction ratio than pile-of-plates polarizers, were used although their transmission efficiency is not particularly high. The experimental results did not in fact, in this case, violate Bell's inequality. The value of η was found to be equal to 0.216 ± 0.013 , whereas on the basis of quantum mechanics $\eta_{qm} = 0.266$. However, it was discovered later that there were stresses in one lens, due to an improper mounting. Such stresses may have caused a systematic error in the experiment. Another criticism is that Holt and Pipkin may have underestimated the solid angle used in their calculation, but the discrepancy has never been fully explained.

iii) Clauser (1976)

Clauser[20] repeated the experiment performed by Holt and Pipkin, discussed above, using the same cascade and same excitation mechanism. However, instead of using the isotope ^{199}Hg and calcite polarizers, the even isotope ^{200}Hg of mercury and pile-of-plates polarizers were used.

Quantum mechanically, it is expected that $\eta_{qm} = 0.2841$ whereas the experimental result gave $\eta = 0.2885 \pm 0.0093$ in violation of Bell's inequality. Clauser[21] also measured the circular polarization correlation and found $\eta = 0.235 \pm 0.025$ which is to be compared with the quantum mechanical prediction $\eta_{qm} = 0.252$. Thus, this result cannot provide a decisive test of Bell's inequality, even though, it is clear that within the limits of experimental error, this result agrees with quantum mechanics.

iv) Fry and Thomson[22] (1976)

Fry and Thomson investigated the two photons of wavelengths 435.8 nm and 253.7 nm emitted in the $7^3S_1 - 6^3P_1 - 6^1S_0$ cascade in the zero nuclear spin isotope ^{200}Hg of mercury. They used pile-of-plates polarizers, consisting of two sets of seven plates symmetrically arranged so as to cancel out the displacements of transverse rays. The experimental value of $\eta = 0.296 \pm 0.014$ was found to be in agreement with the quantum mechanical prediction, $\eta_{qm} = 0.294 \pm 0.007$ and, clearly, violates Bell's inequality.

v) Aspect, Grangier and Roger[23] (1981)

Aspect, Grangier and Roger used the same source as Freedman and Clauser. However, in their case, a dye laser beam tuned to 581 nm was used to excite the calcium atom

to the $4p^2^1S_0$ state by a non-resonant two-photon absorption process. This experiment produced a coincidence rate of about 100 s^{-1} , allowing measurements of 1 % statistical accuracy to be obtained in only 100 s counting time. The experimental value found for η was 0.3072 ± 0.0043 in excellent agreement with the quantum mechanical prediction $\eta_{qm} = 0.308 \pm 0.002$ and violating Bell's inequality by 13 standard deviations.

vi) Aspect, Grangier and Roger [24] (1982)

Aspect, Grangier and Roger also performed an experiment using the same source as described above but with two-channel polarizers instead of the previous one-channel pile-of-plates type. Their results were again in good agreement with quantum mechanics.

vii) Aspect, Dalibard and Roger (1982)

It is important to note that, during the measurements described so far, the polarizers were fixed at various angles for long periods of time. One may then argue that the presence of the polarizers, set at particular angles would allow the source and polarizers to, in some way, sense each others presence via a signal travelling with subluminal speed and therefore influence the outcome of the correlation measurement. To overcome this objection Aspect [25] suggested an experiment, in which the settings of the polarizers were changed in a time which was short

compared with the time of flight of photons from source to each polarizer. Later, Aspect, Dalibard and Roger[26] performed the experiment using the same source as described in section (iii). The result of their experiment also violated Bell's inequality and was in agreement with quantum mechanical theory.

viii) *Perrie, Duncan, Beyer and Kleinpoppen[27] (1985)*

In this unique experiment, the only experiment not involving an atomic cascade, an excited atomic deuterium source was used. The main channel for the spontaneous de-excitation of the $2S_{1/2}$ state of deuterium is by the simultaneous emission of two photons and the results of polarization correlation measurement of the two photons were used to test Bell's inequality. Quantum mechanics predicts that $\eta_{qm} = 0.272 \pm 0.008$. Experimentally, it was found that $\eta = 0.268 \pm 0.010$ in violation of Bell's inequality but in agreement with the quantum mechanical prediction.

§ 1.3 THE NO-ENHANCEMENT HYPOTHESIS

Although the predictions of quantum mechanical theory have given good agreement with all but one experiment, and thus appear to have rendered untenable a local realistic view of the world, it still remains for Bell's inequalities to be tested in ideal form. Clearly, in order to draw any decisive conclusions from the actual experimental results, one has to make a subsidiary assumption, either in the CHSH form[15]: *If a pair of photons emerges from the two polarizers the probability of their joint detection is independent of the orientation of the polarizers' axes*, or, as stated by Clauser and Horne, in the form[14]: *For every atomic emission, the probability of a count with a polarizer in place is not larger than with the polarizer removed*. The assumption in either form is necessary due to the following reasons:

- 1) The detection efficiency of photomultipliers in the ultraviolet and visible part of the spectrum is low.
- 2) The solid angle subtended by the detection system at the source is finite.

Therefore, in practice, only a very small fraction of emitted photon pairs is actually detected. We must then assume that the presence of the polarizers does not

introduce any bias into the detection probability for photon pairs. Although many physicists might regard such an assumption as more or less self evident however, from a purely logical point of view, no experiment to date can be considered to have provided grounds for a completely unequivocal rejection of local realism. Indeed some authors[28-34] have effectively taken the view that the experimental results are strong evidence for the existence of a new physical phenomenon, enhancement, in the detection process.

1.3.1 Local Realistic Models

Many local realistic models invoking enhancement have been suggested. For example recently Marshall and Santos[28] produced a model in which they assumed that the two photons emitted by the source were classical wave-packets with well defined intensities and polarization. They suggested that these weak light signal undergo stochastic changes in intensity, in addition to the normal change in polarization, in their interaction with optical devices. This assumption led to enhancement in the detection probability allowing the results of all two-photon experiments so far performed to be explained in local realistic terms but at the expense of creating small deviations from Malus' law in single photon physics.

More recently Ferrero and Santos[29] produced a local realistic model with enhancement which makes the same prediction as quantum mechanics in all experiments with correlated two-photon pairs. Although their approach is very implausible it does serve to demonstrate clearly that the series of polarization correlation experiments, reviewed in the last section, has not strictly eliminated the possibility of a local realistic explanation of the results and, hence, by its nature, rules out the possibility of an empirical decision being made between quantum mechanics and local realism in this type of experiment.

1.3.2 Proposed Experimental Tests

It follows that because of the serious implications of this debate for our understanding of the nature of reality, it is important to carry out experiments either:

- 1) in situations where a distinction between the predictions of local realism and quantum mechanics exists without the need for additional assumptions, or,
- 2) in situations where the validity of the assumptions themselves may be investigated.

An example of the first approach, where, without the need for any additional assumptions, the predictions of local realistic theories disagree with those of quantum

mechanics, was proposed by Garuccio and Selleri[30]. They showed how, for a certain class of local realistic model, all existing results involving single photon physics and two polarizer experiments could be explained in local realistic terms. Moreover, they also demonstrated that if *an additional polarizer* was inserted in one detection arm of the apparatus, a finite and measurable difference between the predictions of local realism and quantum mechanics should exist. In their approach, in addition to a polarization vector \vec{I} , a detection vector $\vec{\lambda}$ was attributed to each photon of a pair. This detection vector was assumed to be unaffected by passage through linear polarizers. The probability of a detection was however postulated to be dependent on the angle between $\vec{\lambda}$ and \vec{I} . In the conventional arrangement, shown in figure 1.1, this angle of course, changes as the polarizers are rotated relative to each other. Or in other words, a particular mechanism leading to enhancement was assumed. They demonstrated necessary conflict with quantum mechanics in hitherto untested experimental arrangements. For this type of experimental arrangement a model proposed by Marshall and Santos[31] suggested the possibility of a small deviation from the conventional quantum mechanical prediction. Later, using the same basic ideas, Selleri[35] developed inequalities which, in principle, could be tested by inserting half-wave ($\lambda/2$ -wave) plates in the two-polarizer type of experiment just

in front of the photomultipliers D1 and D2, shown in figure 1.1.

Assuming that only the relative orientation of the polarizers' axes is important and that, insofar as it is acceptable to think in terms of individual photons emerging from the polarizers, the polarization state of each photon is determined by the setting of the polarizer through which it has passed, we can express the CHSH form of the assumption as follows: *If a pair of photons emerges from the two polarizers, the probability of their joint detection is independent of the relative angle between the plane of linear polarization of the two photons just prior to detection.* The Garuccio-Selleri approach is based precisely on the denial of this assumption.

§ 1.4 PLAN OF THE PRESENT WORK

In the previous section, the proposed experimental tests of the no-enhancement hypothesis were discussed. These ideas are investigated in the present work by observing the polarization properties of the two-photon emission of atomic deuterium. In addition, the two-photon emission process in the presence of an electric field is studied for the first time. In chapter two, the two-photon state vectors and density matrices describing the two-photon polarization state are constructed, and the quantum mechanical predictions derived. Chapter three deals with the descriptions of the apparatus and experimental techniques. Chapter four displays all the results of the experiments and finally the conclusions are presented in chapter five.

CHAPTER TWO
THEORETICAL ASPECTS

§ 2.1 THE STATE VECTOR AND DENSITY MATRIX REPRESENTATIONS OF THE POLARIZATION STATE OF TWO-PHOTONS

The simplest atom, atomic hydrogen, continues to provide a testing ground for fundamental ideas in atomic physics and quantum mechanics. The two-photon decay of metastable atomic hydrogen was first observed experimentally, at Stirling, by O'Connell et al[36]. Subsequently, Perrie et al[27] studied the linear polarization correlation and the results were used to test Bell's inequality. In the present work the author reports the measurement of the polarization correlations in novel situations to test further quantum mechanics versus local realism and to investigate the no-enhancement hypothesis. First of all, the emission process and the characteristics of the two-photons emitted in the decay of metastable atomic hydrogen are discussed then, in sections 2.1.2 and 2.1.3 respectively, the construction of the state vector is discussed and density matrix approach is developed.

2.1.1 Two-photon Decay of Metastable Atomic Hydrogen

The theory of multi-photon emission was pioneered by Göppert-Mayer[37] in 1931. She predicted the possibility of spontaneous two-photon decay processes. Breit and Teller[38], in 1940, first studied the $2S_{1/2} \rightarrow 1S_{1/2}$ transition in atomic hydrogen. Subsequently, several

authors[39-44] have applied the theory to determine the two-photon decay rate of hydrogenic ions, including relativistic effects[45,46]. A hydrogen atom in the $2^2S_{1/2}$ ($H(2^2S_{1/2})$) state cannot readily decay to the lower energy $1S_{1/2}$ state, the ground state. This is due to the fact that electric dipole and electric quadrupole transitions between these two states are not allowed. The energy level of the $2S_{1/2}$ state, due to the Lamb shift, lies slightly above that of the $2P_{1/2}$ state. Since the energy difference is small, however, the probability of spontaneous emission by a cascade process, involving the sequential emission of two photons, via the $2P_{1/2}$ state, is negligibly small. The lifetime τ of this process is about 5×10^9 s[41]. The $2S_{1/2}$ state can also decay by the simultaneous emission of two electric dipole photons $2E1$ or by the emission of a single magnetic dipole photon $M1$; the latter effect being significant only when relativistic effects are important such as in the case of hydrogenic ions with high atomic number Z . For a hydrogenic ion of low Z , the decay rate is[46] $8.229 Z^4$ s $^{-1}$ for $2E1$ transitions and about $2.496 \times 10^{-6} Z^{10}$ s $^{-1}$ for $M1$ transitions. Therefore, for $H(2S_{1/2})$, the $M1$ transition rate is negligible with $\tau = 4 \times 10^8$ s. whereas the lifetime via the $2E1$ decay is relatively short with $\tau = 0.1215$ s. The contribution to the decay of higher order two-photon multipole modes of decay such as $E1-M2$, $2M1$, $2E2$ etc. are also insignificant[44].

Hence, $H(2S^M)$ decays primarily by the simultaneous emission of two photons with a total energy of 10.2 eV. Figure 2.1 shows the spectral distribution of the two-photon process; each photon can have any energy ranging from 0 to 10.2 eV. The distribution is symmetric about 5.1 eV (243 nm) on an energy scale. It follows that the polarization state of the two-photon process can be analysed in air using relatively simple lenses and pile-of-plates polarizers, whereas all other hydrogenic two-photon decay processes produce photons of higher energy where it is difficult to measure polarization directly.

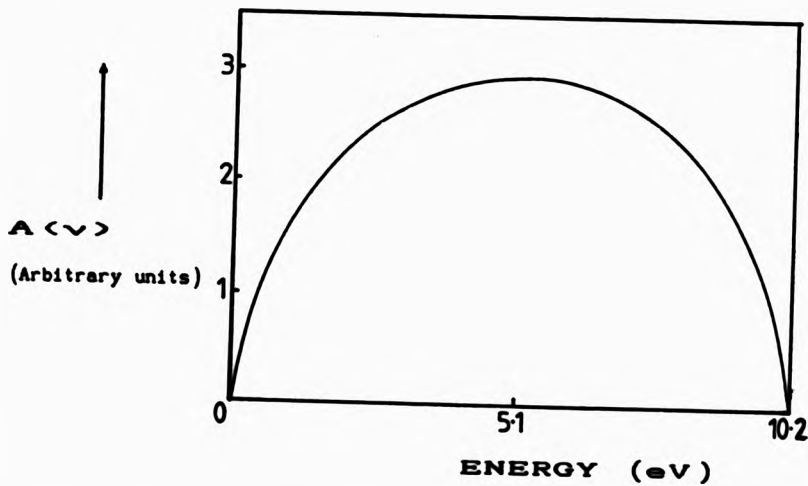


Figure 2.1 Theoretically predicted two-photon spectral distribution for metastable hydrogen.

The two-photon transition can be described theoretically most easily in terms of the scattering operator S which is expanded to second order in terms of the interaction Hamiltonian H_1 between the atomic electron and the radiation field. The matrix element of the second order term between the initial and final state of the atom plus radiation field is then calculated, making use of the interaction Hamiltonian H_1 in the form

$$H_1 = -\frac{e}{m} \vec{p} \cdot \vec{\Lambda} + \frac{e^2 |\vec{\Lambda}|^2}{2m} \quad (2.1)$$

where e is the electronic charge, m is the atomic mass, \vec{p} is the canonical momentum of the electron, and $\vec{\Lambda}$ is the vector potential describing the radiation field, whose direction specifies the polarization of the electric vector. The last term of Eq. (2.1), which is quadratic in $\vec{\Lambda}$, describes processes involving an interchange of two photons. This term is small due to the presence of e^2 and therefore can be neglected. The vector potential $\vec{\Lambda}$ can be written as a superposition of creation and annihilation operators a^+ and a , respectively:

$$\vec{\Lambda} = \sum_{\sigma=1}^2 \sum_n \frac{\hbar}{2\epsilon \omega_n V} \vec{e}_{\sigma n} (a_{\sigma n}^{\dagger} e^{-i\vec{k}_n \cdot \vec{r}} + a_{\sigma n} e^{i\vec{k}_n \cdot \vec{r}}) \dots\dots\dots (2.2)$$

where \vec{e} is a unit vector in the direction of polarization, σ ($= 1, 2$) represents the two polarization states, ϵ is the permittivity of free space, ω_n and k_n the angular frequency and wave vector of the n 'th mode,

and V is the box volume used to ensure proper normalisation. The terms involving the annihilation operator vanish, since there is initially no photon to be annihilated.

By using the above expression for H_1 one can write the matrix element describing the two-photon decay process in the form

$$\frac{e^2}{m^2} \sum_P \frac{\langle F | \vec{p} \cdot \vec{A} | P \rangle \langle P | \vec{p} \cdot \vec{A} | I \rangle}{E_I - E_P} \dots\dots\dots (2.3)$$

where $|I\rangle$, $|F\rangle$ describe the initial state and the final state of the atom and radiation field together and E_I is the energy of the initial state. The summation is taken over all allowed virtual intermediate states $|P\rangle$ of energy E_P . The term $\vec{p} \cdot \vec{A}$ occurs twice in the above equation so that two photons are emitted. If $|\Psi_{2\omega}\rangle$, $|\Psi_{\omega_1}\rangle$, and $|\Psi_{\omega_2}\rangle$ represent the atomic states of energies W_I , W_P and W_F respectively, the state vector $|I\rangle$ can be written as,

$$|I\rangle = |0\rangle |\Psi_{2\omega}\rangle \dots\dots\dots (2.4)$$

where initially, there is no photon in the field and the atom is in the initial state $|\Psi_{2\omega}\rangle$. The state vector of the final state, where in this case two photons are emitted, is of the form

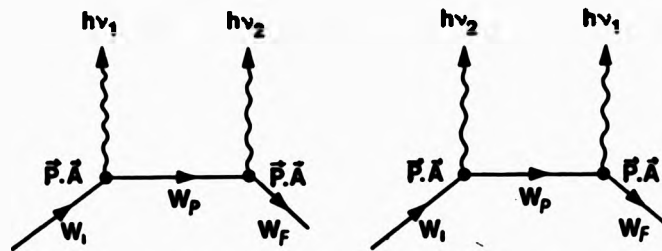


Figure 2.2 Feynman diagrams representing the spontaneous simultaneous emission of two-photons.

$$|F\rangle = |\vec{k}_1, \hat{e}_1\rangle |\vec{k}_2, \hat{e}_2\rangle |\Psi_{1,0}\rangle \quad (2.5)$$

which describes the state in which the two-photons have momentum \vec{k}_1 and \vec{k}_2 corresponding to photon energies $h\nu_1$ and $h\nu_2$ respectively, and the atom is in the state $|\Psi_{1,0}\rangle$. The virtual intermediate state $|P\rangle$ takes the form,

$$|P\rangle = |\vec{k}_1, \hat{e}_1\rangle |\Psi_p\rangle \text{ or } |\vec{k}_2, \hat{e}_2\rangle |\Psi_p\rangle \quad (2.6)$$

The emission process of the two-photons can be illustrated by the Feynman diagrams shown in figure 2.2, which demonstrate that the two-photons can be emitted in *either order* leading to the two terms in the final expression for the probability per second $A(\nu_1)d\nu_1$ for the spontaneous, simultaneous emission of two-photons with one photon in the range $d\nu_1$ in the neighbourhood of frequency ν_1 . Making the dipole approximation and changing from the dipole velocity to the dipole length form of the matrix element we obtain [36]

$$\overline{\Lambda(v_1)dv_1} = K \sum_{\substack{\mathbf{e}_1 \\ \mathbf{e}_2}} \left\{ \frac{\langle \Psi_{1m} | \hat{\mathbf{r}} \cdot \hat{\mathbf{e}}_1 | \Psi_m \rangle \langle \Psi_m | \hat{\mathbf{r}} \cdot \hat{\mathbf{e}}_2 | \Psi_{2m} \rangle}{W_2 - W_m - hv_1} + \frac{\langle \Psi_{1m} | \hat{\mathbf{r}} \cdot \hat{\mathbf{e}}_2 | \Psi_m \rangle \langle \Psi_m | \hat{\mathbf{r}} \cdot \hat{\mathbf{e}}_1 | \Psi_{2m} \rangle}{W_2 - W_m - hv_2} \right\}^2 dv_1$$

..... (2.7)

where the constant $K = 1024\pi^4 e^4 v_1^2 v_2^2 / c^4$,

and the double bar over $\Lambda(v_1)$ indicates that the average is taken over the directions of propagation and over the polarization directions. It is important to note that the system never really assumes the virtual intermediate states and the two-photons are, in fact, emitted simultaneously, although the Feynman diagrams and the theoretical expression for the transition probability suggest that the photons are emitted one after the other. The intermediate states are introduced purely for purposes of the mathematical calculation.

2.1.2 State Vector Representation of the Two-photon Pairs

The state vector of a photon pair emitted, in diametrically opposite directions, from the decay of metastable atomic hydrogen which is in a state of zero angular momentum before and after emission, may be constructed as follows: First, consider figure 2.3, which demonstrates the important transition routes, with

nuclear and electronic spins neglected, since the electric dipole operator is diagonal in nuclear and electronic spin, as pointed out by Breit and Teller[38]. For the processes we are considering, the transition $2S_{1/2} \rightarrow 1S_{1/2}$ involves *no* net angular momentum along the common axis of the photon pair. In addition, the initial and final atomic states are both of *even* parity so that, if \hat{P} is the parity operator for which $\hat{P}|R(1)\rangle = |L(2)\rangle$, $\hat{P}|L(1)\rangle = |R(2)\rangle$ etc. we require $\hat{P}|\Psi\rangle = +|\Psi\rangle$

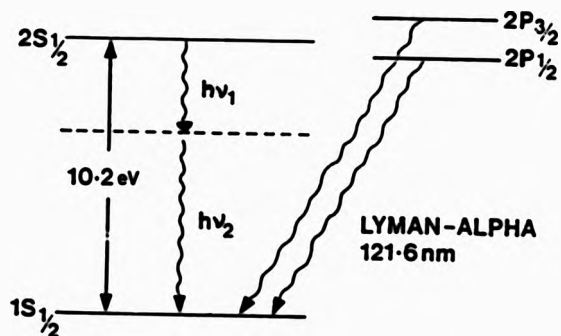


Figure 2.3 Energy level diagram of the first two levels of atomic hydrogen neglecting hyperfine structure (not to scale). The two photons frequency ν_1 and ν_2 can have any energy provided $h\nu_1 + h\nu_2 = 10.2$ eV. The important decay modes are shown.

corresponding to even parity. Thus from parity and angular momentum conservation principles, one can create the two-photon state vector, in a circular polarization basis, as

$$|\Psi\rangle = 1/\sqrt{2} [|R(1)\rangle \otimes |R(2)\rangle + |L(1)\rangle \otimes |L(2)\rangle] \quad (2.8)$$

The state vector above applies also to the two-photon pair emitted from a $J = 0 \rightarrow 1 \rightarrow 0$ atomic cascade. Quantum mechanically, a measurement with circular polarizers, causes the state vector in Eq. (2.8) to collapse into either one of the states $|R(1)\rangle \otimes |R(2)\rangle$ or $|L(1)\rangle \otimes |L(2)\rangle$, each possibility occurring with a probability of a half. For a plane wave, helicity is a good quantum number thus both photons have either negative helicity as in the state $|R(1)\rangle \otimes |R(2)\rangle$ or positive helicity as in state $|L(1)\rangle \otimes |L(2)\rangle$. However, in the case of an *odd* parity system, i.e. for a system in which a change of parity takes place in the transition process, $\hat{P}|\Psi\rangle = -|\Psi\rangle$, the state vector takes the form

$$|\Psi\rangle = 1/\sqrt{2} [|R(1)\rangle \otimes |R(2)\rangle - |L(1)\rangle \otimes |L(2)\rangle] \quad (2.9)$$

which represents, for example, the state vector describing the two-photons emitted in a $J = 1 \rightarrow 1 \rightarrow 0$ atomic cascade, and the singlet state of para-positronium annihilation where the parity of the initial state is odd and the final vacuum state is even.

In the case where the two-photons propagate along + z and - z directions then Eq. (2.8) can easily be transformed into an expression involving the linear polarization basis states, $|x\rangle$ and $|y\rangle$, by using the relations

$$|R\rangle = 1/\sqrt{2} (|x\rangle + |y\rangle) \text{ and } |L\rangle = 1/\sqrt{2} (-|x\rangle + |y\rangle)$$

whence,

$$|\Psi\rangle = 1/\sqrt{2} [|x(1)\rangle \otimes |x(2)\rangle + |y(1)\rangle \otimes |y(2)\rangle] \quad (2.10)$$

The state vector $|\Psi\rangle$, it should be remarked, is invariant with respect to rotation about the propagation or detection axis. It is also important to note that the two-photons described by the state vector $|\Psi\rangle$ above, have an undefined polarization state prior to measurement. By carrying out a measurement with linear polarizers, the state vector collapses to $|x(1)\rangle \otimes |x(2)\rangle$ or $|y(1)\rangle \otimes |y(2)\rangle$, instantaneously when either one of the photons is first analysed and detected, irrespective of the separation between them and of the choice of x or y direction which is arbitrary with respect to rotation about the axis of propagation. Thus, the result of a polarization measurement of the photon by a detector on one side can be considered to determine *instantaneously* the result for the other photon of the pair, despite the fact that the detection events are space-like separated in the relativistic sense.

2.1.3 Density Matrix Representation of the Two-photon Pairs

The state vector which describes the two-photon emission of metastable atomic hydrogen (or deuterium) discussed earlier can also be represented in the matrix formulation (described in detail in the appendix) in the following way (cf. Eq. (2.10))

$$|\Psi\rangle = \frac{1}{\sqrt{2}} \left\{ \begin{bmatrix} 1 \\ 0 \end{bmatrix} \otimes \begin{bmatrix} 1 \\ 0 \end{bmatrix} + \begin{bmatrix} 0 \\ 1 \end{bmatrix} \otimes \begin{bmatrix} 0 \\ 1 \end{bmatrix} \right\} \quad (2.11)$$

and the adjoint state is

$$\langle\Psi| = \frac{1}{\sqrt{2}} \left\{ \langle 1 \quad 0 | \otimes \langle 1 \quad 0 | + \langle 0 \quad 1 | \otimes \langle 0 \quad 1 | \right\} \quad (2.12)$$

In Eqs. (2.11) and (2.12) above and in the following discussions, the matrices describing photon 1 (photon 2) are always placed on the left hand side (the right hand side) of \otimes . Therefore, in the $|x\rangle$ and $|y\rangle$ basis we have the density matrix which describes the two-photon pairs

$$\begin{aligned} \rho &= |\Psi\rangle\langle\Psi| \\ &= \frac{1}{2} \left\{ (|x(1)\rangle\langle x(1)| \otimes |x(2)\rangle\langle x(2)| + |y(1)\rangle\langle y(1)| \otimes |y(2)\rangle\langle y(2)|) \right. \\ &\quad \left. + (|x(1)\rangle\langle x(2)| + |y(1)\rangle\langle y(2)|) \right\} \\ &\dots\dots\dots (2.13) \end{aligned}$$

In the matrix formulation, we have

$$\rho = \frac{1}{2} \left\{ \begin{aligned} & \begin{bmatrix} 1 & 0 \\ 0 & 0 \end{bmatrix} \otimes \begin{bmatrix} 1 & 0 \\ 0 & 0 \end{bmatrix} + \begin{bmatrix} 0 & 1 \\ 0 & 0 \end{bmatrix} \otimes \begin{bmatrix} 0 & 1 \\ 0 & 0 \end{bmatrix} \\ & + \begin{bmatrix} 0 & 0 \\ 1 & 0 \end{bmatrix} \otimes \begin{bmatrix} 0 & 0 \\ 1 & 0 \end{bmatrix} + \begin{bmatrix} 0 & 0 \\ 0 & 1 \end{bmatrix} \otimes \begin{bmatrix} 0 & 0 \\ 0 & 1 \end{bmatrix} \end{aligned} \right\} \dots\dots\dots (2.14)$$

Evaluating the direct product, we obtain

$$\rho = \frac{1}{2} \begin{pmatrix} 1 & 0 & 0 & 1 \\ 0 & 0 & 0 & 0 \\ 0 & 0 & 0 & 0 \\ 1 & 0 & 0 & 1 \end{pmatrix} \dots\dots\dots (2.15)$$

or, similarly, in a circular polarization basis, $|\Psi\rangle$ and $\langle\Psi|$ take the forms, respectively

$$|\Psi\rangle = \frac{1}{\sqrt{8}} \left\{ \begin{bmatrix} 1 \\ -1 \end{bmatrix} \otimes \begin{bmatrix} 1 \\ 1 \end{bmatrix} + \begin{bmatrix} 1 \\ 1 \end{bmatrix} \otimes \begin{bmatrix} 1 \\ -1 \end{bmatrix} \right\}$$

$$\text{and } \langle\Psi| = \frac{1}{\sqrt{8}} \left\{ \langle 1 \quad 1 | \otimes \langle 1 \quad -1 | \right. \\ \left. + \langle 1 \quad -1 | \otimes \langle 1 \quad 1 | \right\}$$

..... (2.16)

These expressions lead to a density matrix ρ which describes the two-photon pairs in circular polarization bases as,

$$\rho = 1/2 \{ |R(1)\rangle\langle R(1)| \otimes |R(2)\rangle\langle R(2)| + \\ |L(1)\rangle\langle L(1)| \otimes |L(2)\rangle\langle L(2)| +$$

$$|R(1)\rangle\langle L(1)| \otimes |R(2)\rangle\langle L(2)| + \\ |L(1)\rangle\langle R(1)| \otimes |L(2)\rangle\langle R(2)|$$

which, equivalently, can be written in the matrix formulation as

$$\rho = \frac{1}{8} \left\{ \begin{bmatrix} 1 & 1 \\ -1 & 1 \end{bmatrix} \otimes \begin{bmatrix} 1 & -1 \\ 1 & 1 \end{bmatrix} + \begin{bmatrix} 1 & -1 \\ 1 & 1 \end{bmatrix} \otimes \begin{bmatrix} 1 & 1 \\ -1 & 1 \end{bmatrix} \right. \\ \left. + \begin{bmatrix} 1 & -1 \\ -1 & -1 \end{bmatrix} \otimes \begin{bmatrix} 1 & 1 \\ 1 & -1 \end{bmatrix} + \begin{bmatrix} 1 & 1 \\ 1 & -1 \end{bmatrix} \otimes \begin{bmatrix} 1 & -1 \\ -1 & -1 \end{bmatrix} \right\} \\ \dots\dots\dots (2.17)$$

which reduces also to the form of Eq. (2.15).

In the above discussions, the density matrix ρ is, of course, normalized such that $\text{Tr}(\rho) = 1$.

§ 2.2 QUANTUM MECHANICAL REPRESENTATION OF ANALYSERS

The two photons under study encounter one or more devices (analysers) which change their state of polarization. This section is devoted to the construction of quantum mechanical operators to represent the *non-ideal* analysers used in the present experimental work. The effect of such devices on the two-photon density matrix (developed in § 2.1) will be discussed in the next section (§ 2.3).

2.2.1 Normal Devices

In quantum mechanics, the action of a device L on a system represented by a state vector $|\psi\rangle$ can be described in terms of an operator I acting on $|\psi\rangle$ to give a new state vector $|\psi'\rangle$. In particular, a polarizer can be represented by a linear operator I with two orthonormal eigenvectors, $|i_1\rangle$ and $|i_2\rangle$, which form a complete set, with non-degenerate eigenvalues i_1 and i_2 . Thus,

$$I|i_1\rangle = i_1|i_1\rangle$$

and

$$I|i_2\rangle = i_2|i_2\rangle$$

..... (2.18)

where i_1 and i_2 are generally complex numbers. In this case, I is a normal operator, in the sense that, it commutes with its adjoint so that

$$[1, 1^\dagger] = 0 \quad (2.19)$$

In terms of $|1_1\rangle$ and $|1_2\rangle$, we can construct projection operators \hat{P}_1 and \hat{P}_2 as follows,

$$\hat{P}_1 = |1_1\rangle\langle 1_1|$$

and

$$\hat{P}_2 = |1_2\rangle\langle 1_2|$$

..... (2.20)

The operators \hat{P}_1 and \hat{P}_2 are thus Hermitian and $\hat{P}_1 + \hat{P}_2 = 1$, where 1 represents the identity operator. Thus, in terms of \hat{P}_1 and \hat{P}_2 which form a complete set, the operator 1 can be written as

$$1 = 1_1\hat{P}_1 + 1_2\hat{P}_2 \quad (2.21)$$

The action of a device, represented by 1, on a beam described by a density matrix ρ is to transform the polarization state of the beam to a new state whose density matrix is ρ' . Where

$$\rho' = 1 \rho 1^\dagger \quad (2.22)$$

The trace operation then yields the final intensity of the beam

$$\begin{aligned} \text{Tr}(\rho') &= |1_1|^2 \text{Tr}(\hat{P}_1 \rho \hat{P}_1) + |1_2|^2 \text{Tr}(\hat{P}_2 \rho \hat{P}_2) \\ &+ |1_1|^2 \text{Tr}(\hat{P}_2 \rho \hat{P}_1) + |1_2|^2 \text{Tr}(\hat{P}_1 \rho \hat{P}_2) \end{aligned}$$

..... (2.23)

The last two terms of the above equation vanish, since the trace of the product of operators is invariant when a

cyclic permutation is performed on these operators (i. e. $\text{Tr}(\alpha\beta\gamma) = \text{Tr}(\beta\gamma\alpha) = \text{Tr}(\gamma\alpha\beta)$) and \hat{P}_1 and \hat{P}_2 form an orthonormal set.

2.2.2 Linear Polarizers

For a linear polarizer, i_1 and i_2 in Eq. (2.18) give the complex amplitudes for transmission for light parallel and perpendicular, respectively, to the transmission axis of the polarizer. It follows that $|i_1|^2 \equiv \epsilon_{\parallel}$ and $|i_2|^2 \equiv \epsilon_{\perp}$, where the quantities ϵ_{\parallel} and ϵ_{\perp} are the transmission efficiencies of the polarizers for light polarized, respectively, parallel to and perpendicular to their transmission axes. For an ideal linear polarizer $|i_1|^2 = 1$ and $|i_2|^2 = 0$.

Now the projection operators of a linear polarizer with transmission axis making an angle θ with x-axis, take the form

$$\hat{P}_1 = \frac{1}{2} \begin{bmatrix} 1 + \cos 2\theta & \sin 2\theta \\ \sin 2\theta & 1 - \cos 2\theta \end{bmatrix}$$

and

$$\hat{P}_2 = \frac{1}{2} \begin{bmatrix} 1 - \cos 2\theta & -\sin 2\theta \\ -\sin 2\theta & 1 + \cos 2\theta \end{bmatrix}$$

..... (2.24)

Hence, on substituting the above expressions for \hat{P}_1 and \hat{P}_2 in Eq. (2.21), we find

$$I = \frac{1}{2} \begin{bmatrix} (I_1 + I_2) + (I_1 - I_2)\cos 2\theta & (I_1 - I_2)\sin 2\theta \\ (I_1 - I_2)\sin 2\theta & (I_1 + I_2) - (I_1 - I_2)\cos 2\theta \end{bmatrix}$$

and

$$I^\dagger = \frac{1}{2} \begin{bmatrix} (I_1^* + I_2^*) + (I_1^* - I_2^*)\cos 2\theta & (I_1^* - I_2^*)\sin 2\theta \\ (I_1^* - I_2^*)\sin 2\theta & (I_1^* + I_2^*) - (I_1^* - I_2^*)\cos 2\theta \end{bmatrix}$$

..... (2.25)

One may also write I in terms of the two dimensional Pauli spinor matrix formulation as,

$$I = \frac{1}{2}(I_0 I + \vec{I} \cdot \vec{\sigma})$$

..... (2.26)

where

$$I_0 = \text{Tr}(I) = I_1 + I_2$$

and

$$\vec{I} = \text{Tr}(I\vec{\sigma})$$

The components of Pauli matrices σ_x , σ_y and σ_z of $\vec{\sigma}$ are defined in the appendix.

The components of \vec{I} are

$$I_x = (I_1 - I_2)\sin 2\theta, \quad I_y = 0,$$

and,

$$I_z = (I_1 - I_2)\cos 2\theta$$

2.2.3 Two Linear Polarizers Placed in Series

Let the system of two linear polarizers placed in series be represented by a quantum mechanical operator I . By

writing Eq. (2.22) in the form of Pauli spinor matrices the following expression for ρ' is obtained,

$$\rho' = \frac{1}{8}(1_0 I + \vec{I} \cdot \vec{\sigma})(I + \vec{P} \cdot \vec{\sigma})(1_0 I + \vec{I} \cdot \vec{\sigma})^\dagger \quad (2.27)$$

where \vec{P} is the Poincaré vector (cf. Eq. (A.25) in the appendix). Evaluation of the product gives

$$\begin{aligned} \rho' = & \frac{1}{8}[1_0 1_0^\dagger + \vec{I} \cdot \vec{I}^\dagger + 1_0 \vec{P} \cdot \vec{I}^\dagger + 1_0^\dagger \vec{P} \cdot \vec{I} + 1 \vec{I}^\dagger \times \vec{I} \cdot \vec{P}] \\ & + \frac{1}{8} \vec{\sigma} \cdot [\vec{I} \cdot \vec{I}^\dagger + 1_0^\dagger \vec{I} + 1 \vec{I} \times \vec{I}^\dagger + 1_0 1_0^\dagger \vec{P} + 1 1_0^\dagger \vec{I} \times \vec{P} \\ & + 1 1_0 \vec{P} \times \vec{I}^\dagger + \vec{I}^\dagger \vec{I} \cdot \vec{P} + \vec{I} \vec{I}^\dagger \cdot \vec{P} - \vec{I} \cdot \vec{I}^\dagger \vec{P}] \\ & \dots \dots \dots (2.28) \end{aligned}$$

Note that the following theorems were used in evaluating the above expression:

$$1) \quad \vec{\alpha} \times (\vec{\beta} \times \vec{\gamma}) = (\vec{\alpha} \cdot \vec{\gamma})\vec{\beta} - (\vec{\alpha} \cdot \vec{\beta})\vec{\gamma} \quad (2.29)$$

$$2) \quad (\vec{\sigma} \cdot \vec{a})(\vec{\sigma} \cdot \vec{b}) = (\vec{a} \cdot \vec{b}) + i\vec{\sigma}(\vec{a} \times \vec{b}) \quad (2.30)$$

Since we are only interested in the intensity, it is necessary to evaluate the trace of ρ' above. We obtain

$$\text{Tr}(\rho') = \frac{1}{4}(1_0 1_0^\dagger + \vec{I} \cdot \vec{I}^\dagger + 1_0 \vec{P} \cdot \vec{I}^\dagger + 1_0^\dagger \vec{P} \cdot \vec{I} + 1 \vec{I}^\dagger \times \vec{I} \cdot \vec{P}) \dots \dots \dots (2.31)$$

noting that $\text{Tr}(\vec{\sigma}) = 0$, and that, hence, terms linear in $\vec{\sigma}$ vanish. For a system consisting of two linear polarizers, B and C, placed in series, we have

$$I = CB \quad (2.32)$$

and by rewriting I , B and C above in Pauli spinor matrix form, the following relations can be established:

$$I_0 = \frac{1}{2} \langle C_0 B_0 + \vec{C} \cdot \vec{B} \rangle$$

and

$$\vec{I} = \frac{1}{2} [B_0 \vec{C} + C_0 \vec{B} + i(\vec{C} \times \vec{B})]$$

..... (2.33)

Let the transmission axes of polarizers B and C make an angle (β) and $(\beta + \alpha)$ with the x -axis, respectively. Then, in the same way as discussed in relation to Eq. (2.26), we find that

$$B_0 = B_1 + B_2,$$

$$B_x = (B_1 - B_2) \sin 2\beta,$$

$$B_y = 0,$$

$$B_z = (B_1 - B_2) \cos 2\beta,$$

$$C_0 = C_1 + C_2,$$

$$C_x = (C_1 - C_2) \sin 2(\beta + \alpha),$$

$$C_y = 0,$$

$$C_z = (C_1 - C_2) \cos 2(\beta + \alpha).$$

..... (2.34)

The quantities I_0 and \vec{I} , in Eq. (2.33) can be rewritten, by virtue of the relations in (2.34) above, in the following way,

$$I_0 = \frac{1}{2} [\langle B_1 + B_2 \rangle \langle C_1 + C_2 \rangle + \langle B_1 - B_2 \rangle \langle C_1 - C_2 \rangle \cos 2\alpha]$$

$$\vec{I} = \frac{1}{2} [\langle B_1 + B_2 \rangle \langle C_1 - C_2 \rangle (\hat{i} \sin 2(\beta + \alpha) + \hat{k} \cos 2(\beta + \alpha))$$

$$+ \langle B_1 - B_2 \rangle \langle C_1 + C_2 \rangle (\hat{i} \sin 2\beta + \hat{k} \cos 2\beta)$$

$$- i \langle B_1 - B_2 \rangle \langle C_1 - C_2 \rangle \hat{j} \sin 2\alpha]$$

..... (2.35)

where \hat{i} , \hat{j} and \hat{k} are unit vectors in cartesian coordinates. Finally, the explicit expression for the intensity of the beam in terms of the parameters of the polarizers can be obtained by substituting Eq. (2.35) in Eq. (2.31), whereupon, we find

$$\begin{aligned} \text{Tr}(\rho') &= \frac{1}{4} \{ S_u S_c + \delta_u \delta_c \cos 2\alpha \\ &+ P_1 [S_u \delta_c \sin 2\beta \cos 2\alpha + \delta_u S_c \sin 2\beta + 2|B_1||B_2|\delta_c \cos 2\beta \sin 2\alpha \cos \varphi] \\ &+ P_2 [2|B_1||B_2|\delta_c \sin 2\alpha \sin \varphi] + P_3 [S_u \delta_c \cos 2\beta \cos 2\alpha \\ &+ \delta_u S_c \cos 2\beta - 2|B_1||B_2|\delta_c \sin 2\beta \sin 2\alpha \cos \varphi] \} \\ &\dots\dots\dots (2.36) \end{aligned}$$

where $B_1 = |B_1| e^{i\theta_1}$, $B_2 = |B_2| e^{i\theta_2}$,
 $S_u = |B_1|^2 + |B_2|^2$, $\delta_u = |B_1|^2 - |B_2|^2$,
 $S_c = |C_1|^2 + |C_2|^2$, $\delta_c = |C_1|^2 - |C_2|^2$,
 and $\varphi = \theta_1 - \theta_2$.

This equation tells us the effect of passing a beam of light through two non-ideal linear polarizers, providing that we know the state of polarization of the incident light (P_1 , P_2 and P_3 defined in the appendix, cf. Eq. (A.25)) and the properties of the polarizers.

2.2.4 Retarder

For a retarder with the fast direction making an angle α with the x-axis the operator R which describes the retardation is

$$R = \begin{bmatrix} \cos\alpha \\ \sin\alpha \end{bmatrix} (\cos\alpha, \sin\alpha) + e^{i\epsilon} \begin{bmatrix} -\sin\alpha \\ \cos\alpha \end{bmatrix} (-\sin\alpha, \cos\alpha) \dots\dots\dots (2.37)$$

The slow direction, perpendicular to the fast direction, is that direction in which the phase is retarded by angle ϵ , where $\epsilon > 0$, and corresponds to the direction of shortened wavelength, and large index of refraction and wave number. In Pauli spinor matrix form, Eq. (2.37) reads

$$R = \frac{1}{2} \{ (1 + e^{i\epsilon}) + (1 - e^{i\epsilon}) (\sigma_x \sin 2\alpha + \sigma_z \cos 2\alpha) \} \quad (2.38)$$

It can be shown that the product of R with its adjoint R^\dagger forms a unitary matrix:

$$RR^\dagger = 1 \quad (2.39)$$

2.2.5 Circular Polarizers

Let a retarder be followed by a linear polarizer, aligned in the x-direction ($\theta = 0$, cf. Eqs. (2.25) and (2.38)). Then, the operator representing the combination is given by

$$iR = \frac{1}{4} [(1_1 + 1_2) (1 + e^{i\epsilon}) + (1_1 - 1_2) (1 - e^{i\epsilon}) \cos 2\alpha]$$

$$\begin{aligned}
 & + \frac{1}{4}[(i_1 - i_2)(1 + e^{i\theta}) + (i_1 + i_2)(1 - e^{i\theta})\cos 2\alpha]\sigma_z \\
 & + \frac{1}{4}[(i_1 - i_2)(1 - e^{i\theta})\sin 2\alpha]i\sigma_y + \frac{1}{4}[(i_1 + i_2)(1 - e^{i\theta})\sin 2\alpha]\sigma_x \\
 & \dots\dots\dots (2.40)
 \end{aligned}$$

In the case of an ideal circular polarizer, one has a $\lambda/4$ -wave plate with a retardation of $\theta = \pi/2$ set with its fast direction at $\alpha = \pi/4$ followed by a perfect linear polarizer for which $i_1 = 1$ and $i_2 = 0$. The above expression then reduces to

$$iR_M = \frac{1}{2} \begin{bmatrix} 1 + i & 1 - i \\ 0 & 0 \end{bmatrix} \quad (2.41)$$

where R_M is the $\lambda/4$ -wave plate operator. The effect of this combination on circularly polarized light is that it allows left hand circularly polarized light to be transmitted but filters out right hand circularly polarized light, hence acting as a left hand circular polarizer. For right hand circularly polarized light the corresponding operator can be written as

$$iR_M = \frac{1}{2} \begin{bmatrix} 1 + i & -(1 - i) \\ 0 & 0 \end{bmatrix} \quad (2.42)$$

In general, when the transmission axis of the linear polarizer is set at angle θ with the x-axis, a perfect circular polarizer can be represented by (cf. Eqs. (2.25))

and (2.38),

$$iR_{\pm} = \frac{1}{4} \begin{bmatrix} (1+i)(1+\cos 2\theta) \pm (1-i)\sin 2\theta & \pm(1-i) \pm (1-i)\cos 2\theta + (1+i)\sin 2\theta \\ \mp(1-i) \pm (1-i)\cos 2\theta + (1+i)\sin 2\theta & (1+i)(1-\cos 2\theta) \pm (1-i)\sin 2\theta \end{bmatrix} \dots\dots\dots (2.43)$$

where the angle $\alpha = \theta \pm \pi/4$. Here iR_{+} represents a left hand circular polarizer and iR_{-} represents a right hand circular polarizer.

§ 2.3 QUANTUM MECHANICAL PREDICTIONS

The quantum mechanical predictions for certain experiments described by the configuration of figure 1.1 are well known. However, there is no theoretical prediction for the experimental set up employed in this work. In this section, detailed quantum mechanical calculations are made to predict the outcomes of the measurements carried out in the present research. The quantum mechanical operators obtained in the last section (§ 2.2) will be applied to the density matrix, developed in § 2.1, describing the two-photon state, to determine the effect of polarizers, rotators and retardation plates on the state of polarization of photons. We shall later compare these quantum mechanical predictions with the actual experimental results of the two-photon polarization correlation measurements described in chapter 4, after substitutions of the measured values of the optical parameters obtained in chapter 3.

2.3.1 Polarization Correlation Analysed by Two Linear Polarizers and a $\lambda/2$ -Wave Plate

To investigate the effects on the polarization correlation measurement of the insertion of an achromatic $\lambda/2$ -wave plate in one detection arm between polarizer B and the adjacent photomultiplier (as shown in figure 4.1)

we calculate as follows; Initially, the incident beam is characterized by the density matrix ρ , developed in § 2.1 (cf. Eq. (2.14)). The polarizers and the $\lambda/2$ -wave plate *transmit* a beam characterized by the density matrix ρ' . Using the operators A and B to denote the effect of linear polarizers A and B, respectively, and letting the effect of the $\lambda/2$ -wave plate be represented by the operator $R_{\lambda/2}$, then the following expression can be written for ρ'

$$\rho' = A \circ R_{\lambda/2} B \rho (A \circ R_{\lambda/2} B)^\dagger \quad (2.44)$$

In practice the transmission axis of polarizer A was aligned fixed along the x-axis, and the fast axis of the $\lambda/2$ -wave plate and the transmission axis of polarizer B were rotated through angles $\theta/2$ and θ , respectively. Therefore, consulting Eq. (2.25) we can write the operators representing polarizer A in the form

$$A = \begin{bmatrix} A_1 & 0 \\ 0 & A_2 \end{bmatrix} \text{ and } A^\dagger = \begin{bmatrix} A_1^* & 0 \\ 0 & A_2^* \end{bmatrix} \quad \dots\dots\dots (2.45)$$

and the operators representing polarizer B as

$$B = \frac{1}{2} \begin{bmatrix} (B_1 + B_2) + (B_1 - B_2) \cos 2\theta & (B_1 - B_2) \sin 2\theta \\ (B_1 - B_2) \sin 2\theta & (B_1 + B_2) - (B_1 - B_2) \cos 2\theta \end{bmatrix}$$

and

$$B^\dagger = \frac{1}{2} \begin{bmatrix} (B_1^* + B_2^*) + (B_1^* - B_2^*) \cos 2\theta & (B_1^* - B_2^*) \sin 2\theta \\ (B_1^* - B_2^*) \sin 2\theta & (B_1^* + B_2^*) - (B_1^* - B_2^*) \cos 2\theta \end{bmatrix} \dots\dots\dots (2.45)$$

We are only interested in the joint probability of detection which is proportional to the trace of the matrix ρ' in Eq. (2.45). Evaluating the trace, by applying the rule of cyclic permutation and knowing that (cf. Eq. (2.39))

$$R_{12} R_{12}^\dagger = 1 \quad (2.47)$$

it follows that the terms involving the operator R_{12} will not appear in the final expression which means in turn that the inserted $\lambda/2$ -wave plate has *no* effect on the polarization correlation measurement. Therefore, *quantum mechanically*, alteration of the relative angle between the plane of polarization of the two photons, just prior to the detection, plays no role in establishing the observed linear polarization correlation. The trace operation of Eq. (2.44) gives us the normalized intensity $R(\theta)/R(\infty)$, where $R(\theta)$ is the intensity as a function of the angle θ and $R(\infty)$ is the intensity measured with the plates of both polarizers removed. In evaluating Eq. (2.44), one has to bear in mind that photon 1 is analysed by polarizer A and photon 2 is analysed by

polarizer B and the $\lambda/2$ -wave plate. Therefore, the operator A is applied *only* to the matrices describing photon 1 (placed on the left hand side of \otimes), whereas the operators B and R_{ω} act on photon 2. By making use of the following theorem

$$\text{Tr} (D_1 \otimes D_2) = (\text{Tr} D_1) (\text{Tr} D_2) \quad (2.48)$$

we can arrive at the following expression

$$\frac{R(\theta)}{R(\omega)} = \frac{1}{4}(\epsilon_{m_1} + \epsilon_{m_2})(\epsilon_{m_1} + \epsilon_{m_2}) + \frac{1}{4}(\epsilon_{m_1} - \epsilon_{m_2})(\epsilon_{m_1} - \epsilon_{m_2}) \cos 2\theta$$

..... (2.49)

where as defined in § 2.2.2, $\epsilon_{m_1} \equiv |A_1|^2$, $\epsilon_{m_2} \equiv |A_2|^2$, ..., etc. Since the insertion of a $\lambda/2$ -wave plate does not play any role in establishing the result, therefore, as expected, the expression above is the same as the one obtained in the literature[27] for the experiment using two linear polarizers alone, apart from the absence of a geometrical factor which takes into account the finite solid half-angle subtended by the collecting lenses at the source. This factor is negligible here (> 0.996) and is, therefore, ignored in establishing the above result and, also, in determining the results of the following calculations.

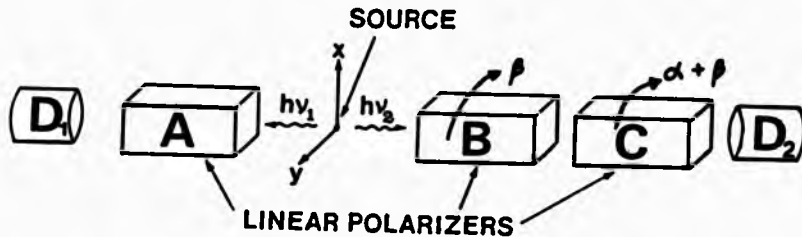


Figure 2.4 The orientation of the polarizers with respect to the x-axis.

2.3.2 Polarization Correlation Analysed by Three Linear Polarizers.

The set up of the experiment using three linear polarizers, A, B and C is shown in figure 2.4. The transmission axis of A is along the x-axis, B makes an angle β with the x-axis and C makes an angle α with B (i.e. $\beta + \alpha$ with the x-axis). The coincidence rate is then proportional to

$$\text{Tr} \rho' = \text{Tr} [A \bullet C B \rho (A \bullet C B)^\dagger] \quad (2.50)$$

Multiplying out $A \rho A^\dagger$ and noting that the operator A acts only on photon 1 so that the matrices describing the polarization state of photon 2 are left undisturbed, we obtain (cf. Eqs. (2.14) and (2.25))

$$\begin{aligned} \rho_{\Lambda}^{\dagger} = \frac{1}{2} & \left\{ \begin{bmatrix} |A_1|^2 & 0 \\ 0 & 0 \end{bmatrix} \bullet \begin{bmatrix} 1 & 0 \\ 0 & 0 \end{bmatrix} + \begin{bmatrix} 0 & A_1 A_2^* \\ 0 & 0 \end{bmatrix} \bullet \begin{bmatrix} 0 & 1 \\ 0 & 0 \end{bmatrix} \right. \\ & + \begin{bmatrix} 0 & 0 \\ A_2 A_1^* & 0 \end{bmatrix} \bullet \begin{bmatrix} 0 & 0 \\ 1 & 0 \end{bmatrix} + \left. \begin{bmatrix} 0 & 0 \\ 0 & |A_2|^2 \end{bmatrix} \bullet \begin{bmatrix} 0 & 0 \\ 0 & 1 \end{bmatrix} \right\} \\ & \dots\dots\dots (2.51) \end{aligned}$$

Evaluating the trace involving photon 1, the second and the third terms on the right hand side of the above equation vanish (cf. theorem (2.48)). Thus we can write

$$\begin{aligned} \text{Tr} \rho & = \frac{|A_1|^2}{2} \text{Tr} \langle \text{CB} \begin{bmatrix} 1 & 0 \\ 0 & 0 \end{bmatrix} B^{\dagger} C^{\dagger} \rangle \\ & + \frac{|A_2|^2}{2} \text{Tr} \langle \text{CB} \begin{bmatrix} 0 & 0 \\ 0 & 1 \end{bmatrix} B^{\dagger} C^{\dagger} \rangle \\ & = \frac{1}{2} \text{Tr} \langle \text{CB} \begin{bmatrix} |A_1|^2 & 0 \\ 0 & |A_2|^2 \end{bmatrix} B^{\dagger} C^{\dagger} \rangle \\ & \dots\dots\dots (2.52) \end{aligned}$$

By comparing the matrix obtained above with the normalized matrix in Eq. (A.27) of the appendix, we find that the components of the Poincaré vector, describing the effective polarization state of the photon analysed by polarizer B, are

$$P_3 = \frac{(|A_1|^2 - |A_2|^2)}{(|A_1|^2 + |A_2|^2)} = \frac{\delta_a}{S_a} \quad \text{and} \quad P_1 = P_2 = 0$$

..... (2.53)

We may consider that the action of the operator A is to change the density matrix describing the state of the polarization of the two-photons from an unpolarized state to a partially polarized state along the x-direction. In order to evaluate the trace of Eq. (2.52), we can immediately use Eq. (2.36) by substituting the values of P_1 , P_2 and P_3 , obtained in Eq. (2.53) above, in Eq. (2.36) and multiplying by $S_a/2$ to obtain $R(\beta, \alpha)$, the actual intensity. We finally obtain

$$R(\beta, \alpha) = \frac{S_a}{8} \langle S_c S_c + \delta_c \delta_c \cos 2\alpha + \frac{\delta_a}{S_a} (S_c \delta_c \cos 2\beta \cos 2\alpha + \delta_c S_c \cos 2\beta - 2|B_1||B_2|\delta_c \sin 2\beta \sin 2\alpha \cos \phi) \rangle$$

..... (2.54)

We are, of course, interested in the normalized coincidence rate which is proportional to the quantity $R(\beta, \alpha)/R(\beta, \pi)$, the ratio of the intensity measured with the three polarizers to the intensity measured with the plates of polarizer C removed (the latter is equivalent to setting $S_c = 2$ and $\delta_c = 0$ in Eq. (2.54)). Hence, the final expression of the normalized coincidence rate in terms of the transmittances of the polarizers may be given as the following

$$\frac{R(\beta, \alpha)}{R(\beta, 0)} = \frac{1}{2}(\epsilon_{m_c} + \epsilon_{m_a}) + \frac{1}{2}(\epsilon_{m_c} - \epsilon_{m_a}) \frac{(\epsilon_{m_a} P - \epsilon_{m_c} Q)}{(\epsilon_{m_a} P + \epsilon_{m_c} Q)} \cos 2\alpha - \Delta(\beta, \alpha)$$

..... (2.55)

where $\Delta(\beta, \alpha)$ is the interference term which takes the form

$$\Delta(\beta, \alpha) = \frac{\sqrt{\epsilon_{m_a}} \sqrt{\epsilon_{m_c}} (\epsilon_{m_a} - \epsilon_{m_c}) (\epsilon_{m_c} - \epsilon_{m_a})}{2(\epsilon_{m_a} P + \epsilon_{m_c} Q)} \sin 2\beta \sin 2\alpha \cos \phi$$

and the quantities P and Q are,

$$P = \frac{1}{2} (\epsilon_{m_a} + \epsilon_{m_c} \cos 2\beta) \quad \text{and} \quad Q = \frac{1}{2} (\epsilon_{m_a} - \epsilon_{m_c} \cos 2\beta)$$

Obviously the term $\Delta(\beta, \alpha) = 0$ for $\beta = 0$ or $\pi/2$. So, for $\beta \neq 0$ or $\pi/2$, the interference term contributes significantly unless $\alpha = \pi/2$ or 0 .

2.3.3 Circular Polarization Analysis

In this experiment, the incident beam, characterized by ρ (cf. Eq. (2.17)) is analysed by a pair of circular polarizers. Each circular polarizer is a combination of a $\lambda/4$ -wave plate and a pile-of-plates linear polarizer (see figure 4.10). Assuming photon 1 is analysed by a right hand circular polarizer (i.e. the fast axis of the $\lambda/4$ -wave plate is set at -45° to the x-axis, and the transmission axis of the linear polarizer (polarizer A) is held fixed at -90° with the x-axis) then, Eq. (2.40) reduces to

$$AR_1 = \frac{1}{2} \begin{bmatrix} A_2(1 + e^{i\theta}) & -A_2(1 - e^{i\theta}) \\ -A_1(1 - e^{i\theta}) & A_1(1 + e^{i\theta}) \end{bmatrix} \dots\dots\dots (2.56)$$

Photon 2 is analysed by a $\lambda/4$ -wave plate, of the same kind as the one in the arm containing polarizer A, followed by polarizer B aligned along the x-axis. The fast axis of this $\lambda/4$ -wave plate is adjusted to make an angle α with the x-axis. The transmitted beam characterized by a density matrix β can be obtained from

$$\beta = A R_1 \rho B R_2 \rho (A R_1 \rho B R_2)^\dagger \quad (2.57)$$

and upon substitutions of ρ (cf. Eq. (2.17)) and the operators AR_1 and BR_2 (cf. Eqs. (2.56) and (2.40), respectively) in the above equation, the trace operation yields

$$\begin{aligned} \text{Tr} \beta &= \frac{1}{4} \langle S_A S_B - \delta_A \delta_B \cos \epsilon_1 - \delta_A \delta_B \sin \epsilon_1 \sin \epsilon_2 \sin 2\alpha \\ &+ \frac{1}{2} \delta_A \delta_B \cos \epsilon_1 (1 - \cos \epsilon_2) (1 - \cos 4\alpha) \rangle \dots\dots\dots (2.58) \end{aligned}$$

from which, it is clear that the probability of joint detection is maximum when we measure right hand circular polarized photons on both sides (in this case, $\alpha = -45^\circ$ and the fast axes of the $\lambda/4$ -wave plates are parallel). The minimum value occurs when we measure right hand circular polarized photons on one side and left hand circular polarized photons on the other (i.e. $\alpha = 45^\circ$ and

the fast axes of the $\lambda/4$ -wave plates are at right angles to each other). $\text{Tr} \hat{\rho} \propto \sin 2\alpha$ only if one uses a perfect $\lambda/4$ -wave plate, (i. e. ϵ_1 and $\epsilon_2 = \pi/2$). However, if we choose, for instance, to rotate polarizer B through an angle θ , whereas the orientation of the transmission axis of polarizer A is held fixed along the x-axis and the fast axes of the $\lambda/4$ -wave plates are also held fixed, then we can write

$$\text{Tr} \hat{\rho} = \frac{1}{4} \langle S_A S_B + \delta_A \delta_B \cos(\epsilon_1 + \epsilon_2) \cos 2\theta \rangle \quad (2.59)$$

where the fast axes of the $\lambda/4$ -wave plates R_1 and R_2 are set at -45° and 45° to the x-axis, respectively. In this case, the probability of joint detection is a maximum when $\theta = 0^\circ$ (the transmission axes of both polarizers parallel and along the x-axis) and a minimum when $\theta = 90^\circ$ (the transmission axes of both polarizers are mutually perpendicular).

Comparing Eqs. (2.58) and (2.59) it is interesting to note that for imperfect polarizers and retarders, rotating the retarder is not equivalent to rotating the linear polarizer.

CHAPTER THREE
EXPERIMENTAL WORK

This chapter is devoted to the experimental details. A description of the apparatus is given in the first section. The second section describes the experimental techniques employed in the present work, carried out on an existing two-photon decay apparatus, with some essential modifications and additions.

§ 3.1 APPARATUS

The experimental arrangement is shown in schematic form in figure 3.1. The main modifications and additions made were

- 1) The mountings were designed so that the polarizers could be rotated without the need to turn off the high voltage applied to the photomultipliers, thus allowing measurements at various different angles to be carried out more easily and efficiently.
- 2) The design and insertion of plates to allow an electric field to be applied in a direction normal to the atomic beam motion at the observation region. This modification permitted the effect of an electric field on the emission process and the polarization correlation of the two-photons to be investigated.
- 3) An additional pile-of-plates linear polarizer, identical to the existing ones, was constructed.
- 4) The system stability was improved by using a much larger deuterium cylinder (5 litres at 600 psi).

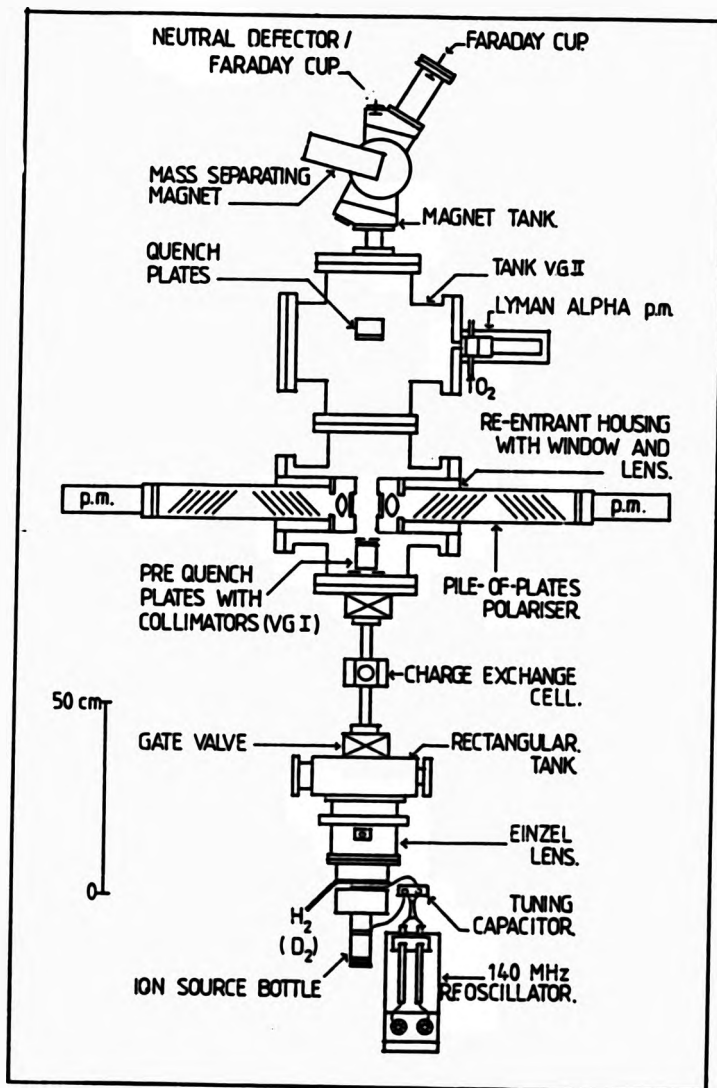


Figure 3.1. Schematic diagram of the apparatus.

Thereby, the operation of the ion source was stabilized by maintaining the pressure of the deuterium supplied to the palladium leak constant at 50 psi. In this way continuous operation of the system, could be achieved for several months without a significant change in the operating conditions.

3.1.1 The Production of the Metastable Atomic Beam

Deuterons extracted from a radio-frequency ion source were focussed by an einzel lens into a cesium charge-exchange cell thus producing (a fraction) an excited beam of atomic deuterium with about 25% in the excited 2S state.

The beam then passed through three sets of electric field plates, the first set being used to quench the beam prior to its entering the observation region, the second set, which was normally removed except when studying the effect of an electric field, being used to apply an electric field in the observation region, and the last set being used to quench the metastable atoms to obtain the Lyman-alpha signals, which provided the basis of the normalization procedure. The main components of the system used to produce and manipulate the metastable beam will now be discussed in more detail.

a) Ion source

A Thoneman type radio-frequency ion source (High Voltage Engineering Corporation, Model C-SO-173) was used to produce deuterons. A 200 watt, 140 MHz self-exciting oscillator (B-TE-78 containing two 4CX 250B air cooled electron tubes) was used to excite the discharge. The base of the source bottle was fitted with a stainless steel lined aluminium canal, surrounded by a quartz bush. A maximum deuterium ion current of ≈ 2 mA, corresponding to 35 keV beam energy (30 keV acceleration and 5 keV probe), was attainable. The flow rate of the deuterium, from a cylinder (5 litres at 600 psi), was controlled by a palladium leak. The ion source could be operated for several months at low energies (≈ 850 eV) with very stable output, after which the canal and the quartz bush needed replacement. To determine the nature of the source output a C-type electromagnet ($B = 0.05$ Tesla) was used to mass analyse the ions at the end of the apparatus.

b) Cesium cell

The cesium charge-exchange cell used is similar to that designed by Bacal et al(47), which achieves a low loss rate of cesium, $\approx 6 \times 10^{-4}$ gm hour⁻¹. The evaporated cesium condenses on the cell walls which are lined with stainless steel mesh, then continuously returns to the central region, thus circulating in a closed cycle by

capillary action. In practice, a 5 gm ampoule of cesium lasts a few months.

c) Electric field plates

In order to monitor metastables, a system consisting of a set of four plates (see figure 3.2) was designed, similar to that of Spiess *et al*[48]. The inner plates, 31×65 mm², spaced 40 mm apart, are biased at opposite potentials with respect to earth. The outer plates, also biased at opposite potentials with respect to earth, are 31×69 mm², extended 4 mm longer than the inner ones to reduce the fringe fields so that the metastables are not quenched prior to entering the observation region. The gap between the plates is 3 mm. A voltage of ± 250 V was permanently applied to these plates. Another set of four plates was designed to study the effect of an electric field on the two-photon emission process. The dimensions of these plates are one third of the ones used for quenching the metastable component of the beam, described earlier.

3.1.2 Optical Systems

One of the critical factors in the design of a decisive experiment to test Bell's Inequality is the absolute transmission of a polarizer for light polarized in the

plane of incidence; therefore, pile-of-plates polarizers were used.

a) Pile-of-plates polarizers

A pair of polarizers was employed in the previous experiment[46] (polarizer A and polarizer B), each polarizer consisting of 12 Suprasil plates, with a short wavelength cut-off at 160 nm. Each plate had a dimension of $100 \times 60 \times 2$ mm and was polished to 2λ per face at $\lambda = 243$ nm. The plates were set at an angle of 56.5° to the direction of the incident light, which is the Brewsters angle for radiation of wavelength $\lambda = 243$ nm. In one of the present experiments, three polarizers were needed. Hence, another polarizer (polarizer C), almost identical to the existing ones was constructed. The transmission of each of these polarizers is higher than 0.9 and, therefore, they could be used for testing Bell's Inequality.

b) Retarders

A $\lambda/2$ -wave plate was used to test the no-enhancement hypothesis. For circular polarization correlation measurements, a combination of the pile-of-plates linear polarizers and two achromatic $\lambda/4$ -wave plates which operate in the spectral range 180 - 320 nm with a retardation accuracy of $\pm 10^\circ$ (for a ray orientated at an angle of $\pm 1^\circ$ to the normal) were used. However, in

practice, the light rays from the source could be at an angle of up to $\pm 2^\circ$ to the detection axis further reducing the retardation accuracy. This system considerably reduced the overall transmission efficiency, due to reflection loss.

3.1.3 Vacuum System

There were three main stainless steel chambers:

- 1) Rectangular tank.
- 2) Vacuum Generator Chamber 1 (VG1).
- 3) Vacuum Generator Chamber 2 (VG2).

The rectangular tank was evacuated by a 6-inch diffusion pump and backed by a rotary pump (Edwards, ED660). The chambers, VG1 and VG2, were each pumped by an 8-inch diffusion pump, connected to a backing pump (rotary pump model ISC 450B). All diffusion pumps were from Edwards (model E06), and fitted with water cooled chevron baffles. Santovac 5 pumping fluid was used. The pressure in all these chambers was $\approx 10^{-7}$ Torr, measured by two ionization gauge heads (VIG 21), one in the rectangular tank and the other in VG2.

3.1.4 Lyman-Alpha Detection System

The Lyman-alpha ($L\alpha$) radiation ($\lambda = 121.6 \text{ nm}$) was detected by a photomultiplier tube (EMR 542 G-08-18, spectral response 105-220 nm) with a LiF window, coupled

to a slow shaping amplifier (NE 4603) and integral discriminator (NE 4623). The discriminator output was fed to a rate meter and a scaler. An additional LiF window into the vacuum system was covered by a 3 mm diameter aperture to allow a statistically adequate $L\alpha$ radiation rate to be monitored. Dried oxygen gas, acting as a filter for the $L\alpha$ photons, was allowed to flow between the LiF vacuum window and the photomultiplier tube.

3.1.5 Data Acquisition System

The coincidence signal was detected by two fast linear focussed tube photomultipliers (EMI, type 9883QA and 9883QB). The spectral response of these photomultiplier (PM) tubes are in the range 180 - 600 nm with a quantum efficiency $\eta = 28\%$ at $\lambda = 420$ nm. The anodes were AC coupled and the photocathodes were operated at ground potential. The pulses generated by the photomultipliers were fed to fast amplifiers (LRS 333) with a maximum gain of $\times 10$ and risetime of 2 ns. The output pulses were then connected to constant fraction (C.F.) differential discriminators (Ortec 583). The output of one of the discriminators (DISC) was used to START a time-to-amplitude converter (TAC) and the other was taken through a variable electronic delay to the STOP input. Finally, the TAC output pulse, whose amplitude was proportional to the time difference between the arrivals of the start and stop pulses, was connected to the input of a multichannel

pulse height analyser (C Canberra 8000). Figure 3.2 demonstrates schematically the detection system described above.

3.1.6 System Interlock

An interlock control unit was incorporated in the system which would completely shut down the system in the event of any of the conditions listed below occurring

- 1) Electric power failure.
- 2) Rise in pressure (vacuum failure).
- 3) Failure of the cooling water supply to the diffusion pumps.
- 4) The Faraday cage housing the Radio-frequency source, which floats at high voltage, is opened.

The radio-frequency source can be operated only when the vacuum is satisfactory, the diffusion pumps are cooled and to protect personnel from high voltage shock, the Faraday cage is closed.

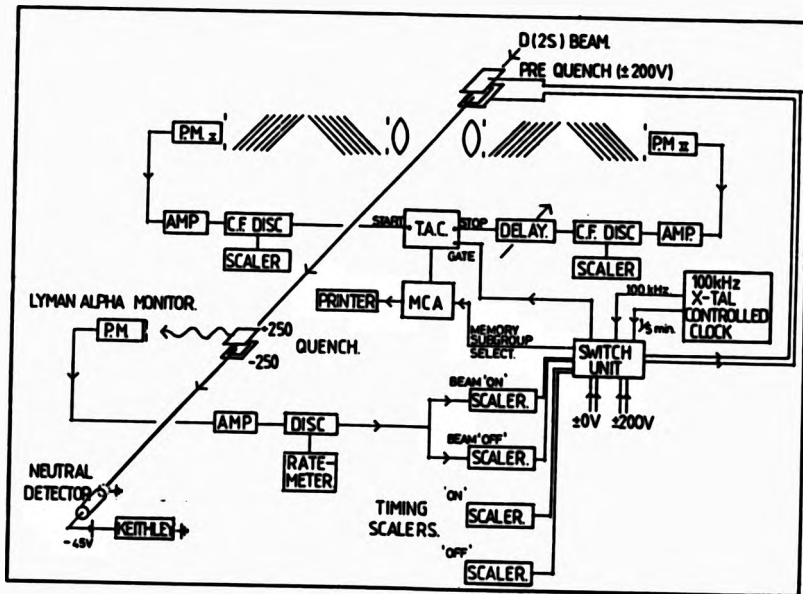


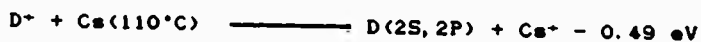
Figure 3.2. Schematic diagram of the detection system.

§ 3.2 EXPERIMENTAL TECHNIQUES

In this section, we propose to explain the experimental techniques employed in this work.

3.2.1 The Production of the Metastable Atomic Deuterium Beam

An excited atomic deuterium beam was used instead of hydrogen (protium) as the source. This is because the former produces relatively less noise, larger deuteron fraction ($\approx 90\%$) and a lower fraction of the molecular ions D_2^+ and D_3^+ . A 850 eV beam of deuterons extracted from the radio-frequency ion source was allowed to pass through cesium vapour, thus creating, by near resonant charge exchange, excited atomic deuterium with approximately 25% of the deuterons being neutralized into the 2S state. The process may be described by the following expression



The cesium cell is heated to $\approx 110^\circ C$ and the temperature at the extremities of the cell is maintained at $\approx 37^\circ C$, to prevent solidification (the melting point of cesium is $28.6^\circ C$), by temperature-controlled circulating water.

3.2.2 Determination of the Optical Parameters

In determining the properties of the imperfect polarizers, auxiliary polarizers and interference filters were placed in the beam of an Hg light source to produce a very high degree of polarized monochromatic light and thus, the transmittances of the unknown polarizers can be measured directly.

a) The transmittances of imperfect polarizers

The value of ϵ_m (ϵ_m) of a polarizer can be obtained by taking the ratio of the intensity of the beam with the transmission axis of the polarizer aligned in the x-direction $I(0^\circ)$ (y-direction, $I(90^\circ)$), to that with the plates removed $I(\infty)$. Hence, we can write

$$\epsilon_m = \frac{I(0^\circ)}{I(\infty)} \quad \text{and similarly} \quad \epsilon_m = \frac{I(90^\circ)}{I(\infty)}$$

It is important to note that, in measuring ϵ_m and ϵ_m , the measured intensity is a combination of a coherent and an incoherent beam of light. The production of an incoherent light beam was a direct result of multiple reflections incurred by the beam in its passage through the pile-of-plates polarizer. The surface of each polarizing plate was polished to only 2λ , thus inducing random phase shifts in the reflected light, thereby producing an incoherent, reflected light beam with respect to the transmitted light beam. Moreover, variable path length is

introduced to the reflected beam because polarizing plates are parallel to the neighbouring plates only to within $\approx \pm 0.2^\circ$. The diameter of the aperture of the photocathode sets a limit on the detectability of n^{th} order reflected light. In this experiment, the diameter of the photocathode allowed only first order reflected light to be of any significance with respect to the experimental results.

Measurements of the transmittance of polarizer B were carried out as follows: With two polarizers, A and B, in situ, the photomultiplier in the arm which contains polarizer A was removed and replaced by two 254 nm interference filters and two ultra violet dichroic linear polarizers which are insensitive to the degree of collimation of the beam (Polacoat 40; $\epsilon_{m1} = 0.3$ and $\epsilon_{m1} = 0.01$, and Polacoat 105; $\epsilon_{m2} = 0.4$ and $\epsilon_{m2} = 0.003$). The transmission axes of both dichroic polarizers and the first pile-of-plates polarizer (polarizer A) were aligned along the x-direction. The radiation from the mercury lamp was focussed by an $f/1$ bi-convex lens of focal length $f = 15$ cm on a ground fused silica plate to produce a diffused diverging light source. Another similar lens was used to collect the beam and subsequently adjust the collimation of the beam to obtain maximum intensity at the photomultiplier tube. In this condition, an image is formed at the photocathode and a

secondary diverging source of light is formed in the region normally occupied by the atomic beam, hence simulating the actual experimental situation, in which light is emitted from the atomic beam. The appropriate convergence of the light in polarizer B (which is being analysed) is thus assured. The degree of polarization P of the beam emerging from polarizer A can be calculated as follows

$$P = \frac{\epsilon_{m_1} \epsilon_{m_2} \epsilon_{m_A} - \epsilon_{m_1} \epsilon_{m_2} \epsilon_{m_A}}{\epsilon_{m_1} \epsilon_{m_2} \epsilon_{m_A} + \epsilon_{m_1} \epsilon_{m_2} \epsilon_{m_A}} > 0.998 \quad (3.1)$$

which is almost perfectly x-polarized light. The transmittance of polarizer A was measured in the same way except that the Hg light source along with the dichroic polarizers and the interference filters were placed in the other arm. The transmittance of polarizer C was measured by inserting polarizer C in between polarizer B and the adjacent photomultiplier tube. The transmission axes of the two dichroic polarizers (placed in the arm containing polarizer A) and polarizer A were aligned along the x-direction. Figures 3.3 - 3.5 show the transmittances of polarizers A, B and C as a function of θ , where θ is the angle between the transmission axes of the polarizers and the x-direction. The values of ϵ_m and ϵ_n of the polarizers A, B, and C are tabulated in Table 3.1.

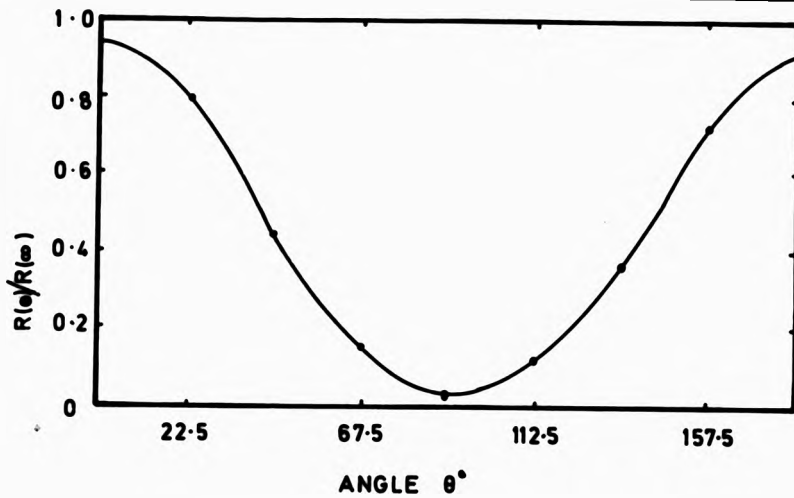


Figure 3.3. The transmittance of polarizer B as a function of θ , where θ is the angle between the transmission axis of polarizer B and the x-direction.

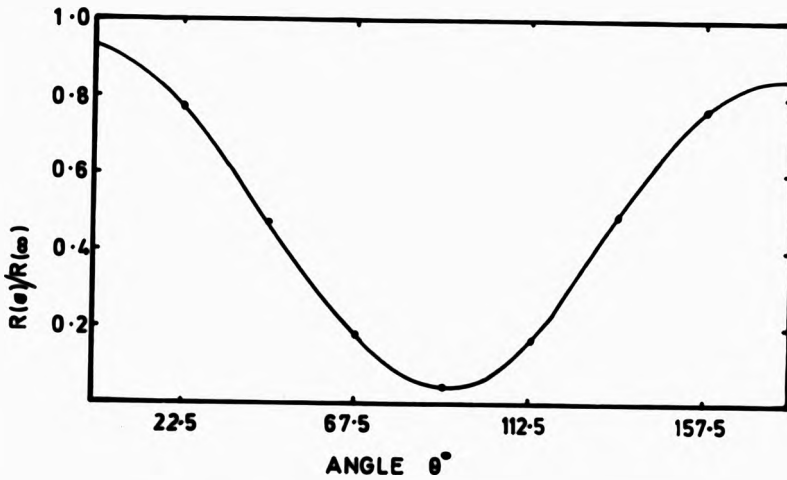


Figure 3.4. The transmittance of polarizer A as a function of θ , where θ is the angle between the transmission axis of polarizer A and the x-direction.

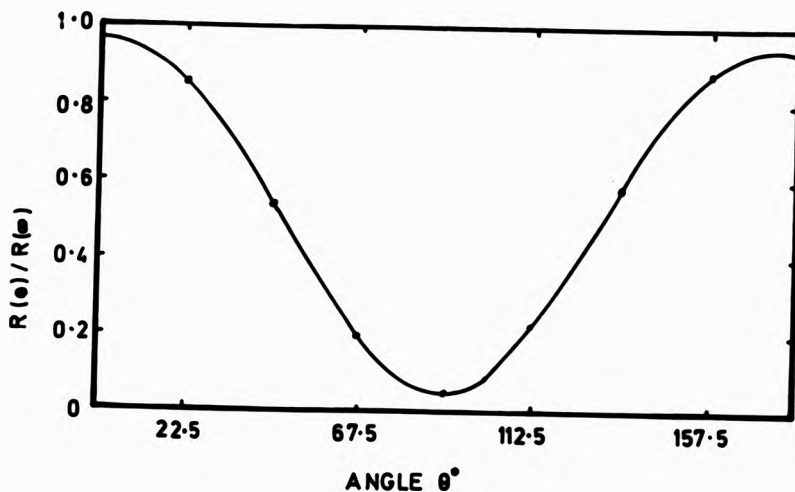


Figure 3.5. The transmittance of polarizer C as a function of θ , where θ is the angle between the transmission axis of polarizer C and the x-direction.

Table 3.1

Transmittances of the polarizers

$\epsilon_{m_A} = 0.9364 \pm 0.0076$	$\epsilon_{m_B} = 0.0314 \pm 0.0006$
$\epsilon_{m_B} = 0.9364 \pm 0.0076$	$\epsilon_{m_C} = 0.0314 \pm 0.0006$
$\epsilon_{m_C} = 0.9665 \pm 0.0009$	$\epsilon_{m_D} = 0.0434 \pm 0.0008$

In the case of the two photon experiment, the transmittances of the polarizers obtained above must be corrected to take into account the absorption in the Suprasil in the region below $\lambda = 243$ nm (by a factor, 908/936 for ϵ_m and 299/320 for ϵ_m).

Another experiment was conducted to investigate the effects of the interference filters and to ensure that only the intensity of $\lambda = 254$ nm radiation contributed to the experimental results obtained. In this experiment, the photomultiplier was replaced by a spectrometer. The result was satisfactory.

b) Determination of the interference factor

Setting up the system in the same way as to measure the transmission of polarizer C, discussed earlier, the variation of the intensity was studied as polarizer B and polarizer C were rotated through angles β and $\alpha + \beta$ with respect to the x-direction, respectively. Since the radiation is x-polarized (cf. Eq. (3.1)), P_1 and P_2 of Eq. (2.36) can be ignored. Whence, upon substitution of the values found in Table 3.1, Eq. (2.36) reduces to

$$\frac{R(\beta, \alpha)}{R(\beta, \varphi)} = 0.505 + \frac{0.202 \cos 2\beta \cos 2\alpha}{\{0.468 + 0.410 \cos 2\beta\}} - \Delta(\beta, \alpha)$$

$$\text{where } \Delta(\beta, \alpha) = \frac{0.1426 \sin 2\beta \sin 2\alpha}{\{0.468 + 0.410 \cos 2\beta\}}$$

$$\text{and } \cos \varphi = 1.$$

Figure 3.6 shows the variation of the intensity as a function of the angle α while the angle β was fixed at 33° and 67.5° from which we obtain the average value of $\Delta(67.5^\circ, 145^\circ) = 0.1975 \pm 0.0525$ which is significantly smaller than the expected value, $\Delta(67.5^\circ, 145^\circ) = 0.2831$, obtained from the above equation. This low effective value of $\Delta(\beta, \alpha)$ can be explained by the fact that only the coherent part of the beam contributes to the interference term and the coherency of the beam is partially destroyed by multiple reflections occurring as the beam passes through the pile-of-plates polarizers, as previously discussed. Figure 3.7 shows three dimensional plots of the variation of the intensity of x-polarized Hg light as a function of the angles α and β .

3.2.3 Optimum Conditions

a) Optimization of signal to noise ratio

The signal to noise ratio of each run was found to be best when the energy of the beam was = 850 eV, and the pressure at the rectangular tank was = 5×10^{-6} Torr. This can be achieved by controlling the flow rate of deuterium gas into the ion source bottle by adjusting the temperature of the palladium leak.

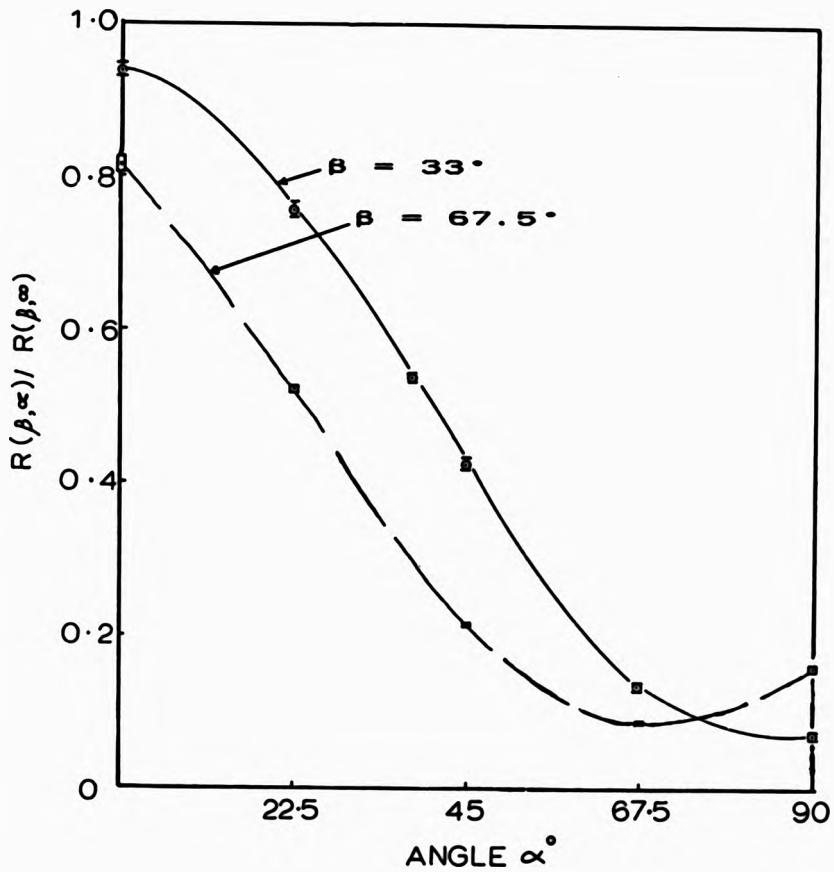


Figure 3.6. The variation of the intensity as a function of the angle α while the angle β was fixed at 33° and 67.5° .

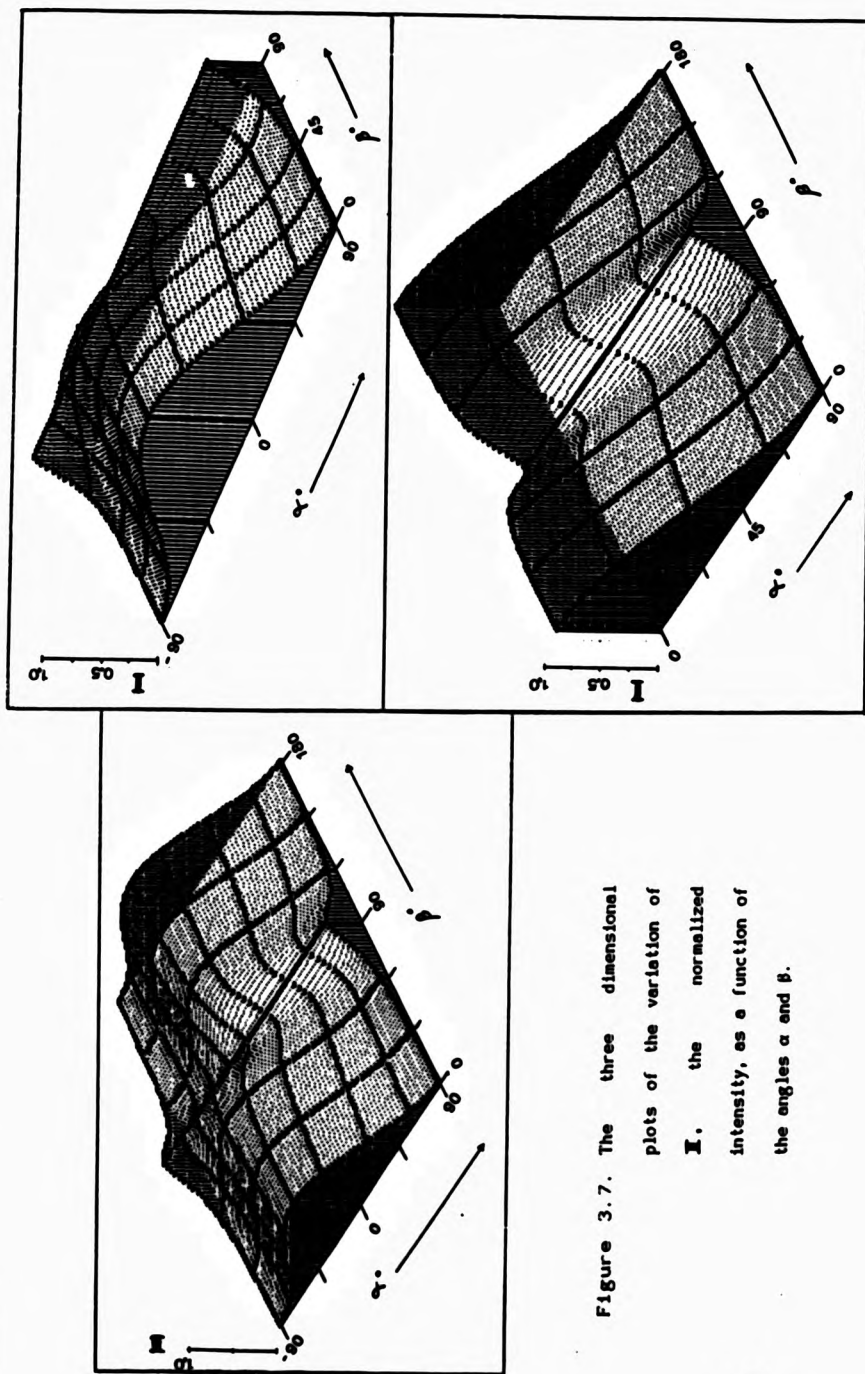


Figure 3.7. The three dimensional plots of the variation of I , the normalized intensity, as a function of the angles α and β .

b) Focussing condition

Throughout the run, the Lyman-alpha rate ($\dot{L}\alpha$) was recorded on a scaler which was in turn connected to a chart recorder, to monitor if there was any significant drift in the count rate. The focussing voltage was adjusted such that $\dot{L}\alpha \approx 1/2 \dot{L}\alpha(\text{maximum})$, to ensure the validity of the normalization procedure. This was necessary since, $L\alpha$ radiation rate was found to be no longer linearly proportional to the observed two-photon coincidence signal when the beam was strongly focussed. This result is in agreement with the suggestion made by Perrie[46].

3.2.4 The Method of Gathering Data

It was important to monitor all experimentally relevant parameters; beam energy, focussing condition, the integrated $L\alpha$ counts, the neutral beam current, the oxygen flow rate to the $L\alpha$ monitor and pressure in the vacuum chamber (rectangular tank). To achieve an acceptable statistical accuracy, data had to be collected typically for about 24 hours for each run.

a) Normalization procedure

The two-photon signal should be proportional to the metastable density. In order to cancel out the effect of the variation of the metastable density from run to run,

the coincidence rate of each run was normalized to a typical $L\alpha$ count rate.

b) Background coincidence rate

Spurious true coincidences are detected, most probably due to cosmic rays, radioactivity and electrical pick up which depend primarily on the physical separation between the two photomultipliers. Cosmic rays are known to produce large amplitude pulses therefore differential constant fraction discriminators were used which effectively reduced this contribution to the background. The two photon coincidence rate was almost always considerably larger than that of the background except when the polarizers' axes were orthogonal. Figure 3.8 displays a typical coincidence spectrum.

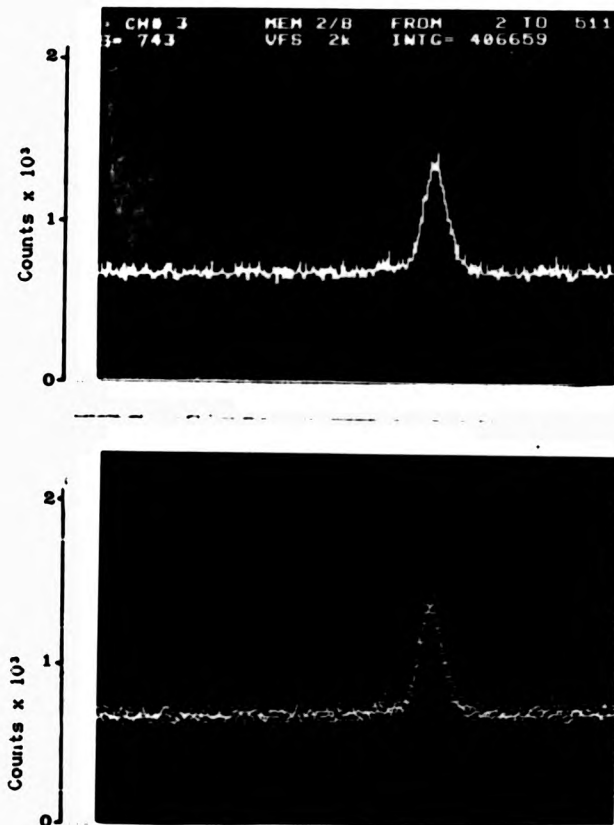


Figure 3.8. A typical coincidence spectrum. Total collection time is 165 hours. The peak FWHM = 27 channels, equivalent to 3 ns, approximately equal to the timing resolution of the electronic detection system.

CHAPTER FOUR

RESULTS

The results of the experimental measurements obtained during the course of the study embodying this thesis are presented in this chapter.

§ 4.1 TWO LINEAR POLARIZERS AND A HALF-WAVE PLATE

This experiment was an attempt to test the no-enhancement hypothesis. Testing this hypothesis was necessary since, as discussed earlier, the efficiencies of the detectors used were rather low, and hence, one could claim that an unrepresentative sample of photon pairs emitted by the source was detected.

1) Measurements

Two experiments were performed in which an achromatic $\lambda/2$ -wave plate was placed on one side of the detection system between one of the linear polarizers (polarizer B) and the adjacent photomultiplier. The arrangement of the detection apparatus is shown schematically in figure 4.1. In the first experiment, the orientation of polarizer A, with its axis aligned in the x-direction, was held constant while polarizer B and the $\lambda/2$ -wave plate in the other arm were rotated. When polarizer B was rotated through an angle θ , where θ is the angle between the transmission axis of polarizer B and the x-axis, the fast axis of the $\lambda/2$ -wave plate was rotated through $\theta/2$, half the angle of rotation of the transmission axis of

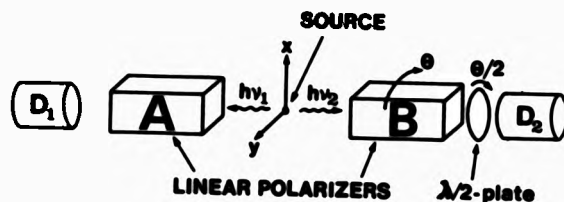


Figure 4.1. Schematic diagram of the $\lambda/2$ -wave plate and two polarizer experiment.

polarizer B. This procedure, ensured that, thinking in terms of photons emerging from polarizers, the orientation of the planes of the polarization of the two photons were *always parallel* just prior to detection in the photomultipliers as the rotation of polarizer B and the $\lambda/2$ -wave plate took place. Coincidence rates, $R(\theta)$, were measured at angles $\theta = 0^\circ, 22.5^\circ, 45^\circ, 67.5^\circ$ and 90° . In the second experiment, the transmission axes of the linear polarizers were kept parallel, aligned with the x-axis. Coincidence rates were then measured as the fast axis of the $\lambda/2$ -wave plate was rotated through angles from 0° to 90° with respect to the x-axis. Thus by passage through the $\lambda/2$ -wave plate the orientation of the plane of linear polarization of the photon changes before impinging on the photomultiplier.

Finally, the singles rate in the detection arm containing the $\lambda/2$ -wave plate was recorded as a function of the orientation of the fast axis of the $\lambda/2$ -wave plate with the orientation of the axis of polarizer B fixed at $\theta = 0^\circ$. This measurement was to check whether there was any residual lack of cylindrical symmetry about the observation axis, resulting either from lack of isotropy in the source itself or in the windows or cathodes of the photomultipliers.

4.1) Results

Figures 4.2 - 4.4 display the experimental results. The plotted coincidence rates were normalized to $R(\infty)$, the coincidence rate obtained with the plates of both linear polarizers removed. The result, given in figure 4.2, agrees with the quantum mechanical prediction, established in § 2.3 (cf. Eq. (2.49)). Figure 4.3 shows the result of the second experiment where the transmission axes of the linear polarizers were kept parallel and the fast axis of the $\lambda/2$ -wave plate was then rotated. These measurements confirm, within the limits of experimental error, that the relative angle between the planes of polarization of the two photons just prior to detection does not contribute any effects to the measured polarization correlation. The result of the singles rate measurement, to check the cylindrical symmetry about the

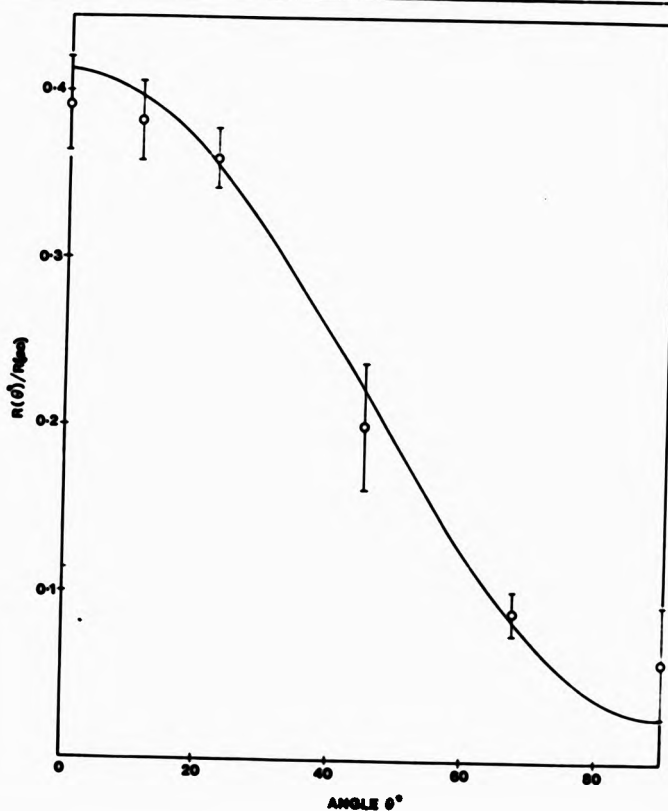


Figure 4.2. The variation of the normalized coincidence signal $R(\theta)/R(\pi/2)$, where $R(\theta)$ is the coincidence rate as a function of θ , the angle between the transmission axis of polarizer B and the x-direction. The fast axis of the $\lambda/2$ -wave plate was rotated through angle $\theta/2$. The quantity $R(\pi/2)$ is the coincidence rate obtained with the half-wave plate in place and the plates of both linear polarizers removed. The solid curve represents the quantum mechanical prediction.

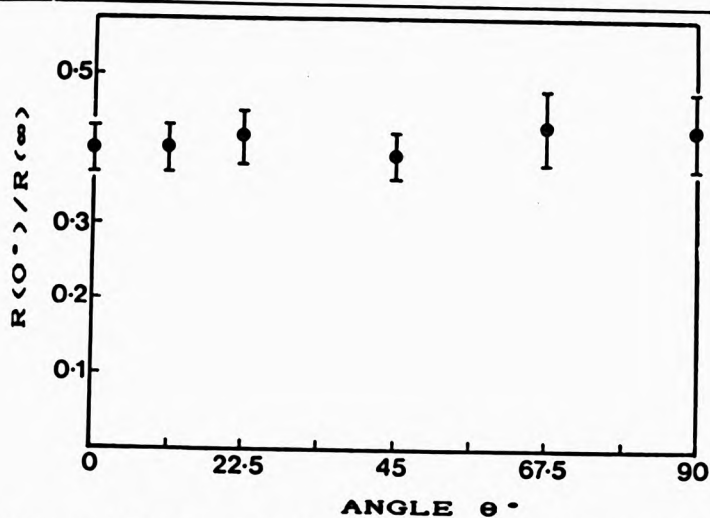


Figure 4.3. The variation of the normalized coincidence signal $R(0^\circ)/R(\infty)$ as the fast axis of the $\lambda/2$ -wave plate was rotated through angle θ .

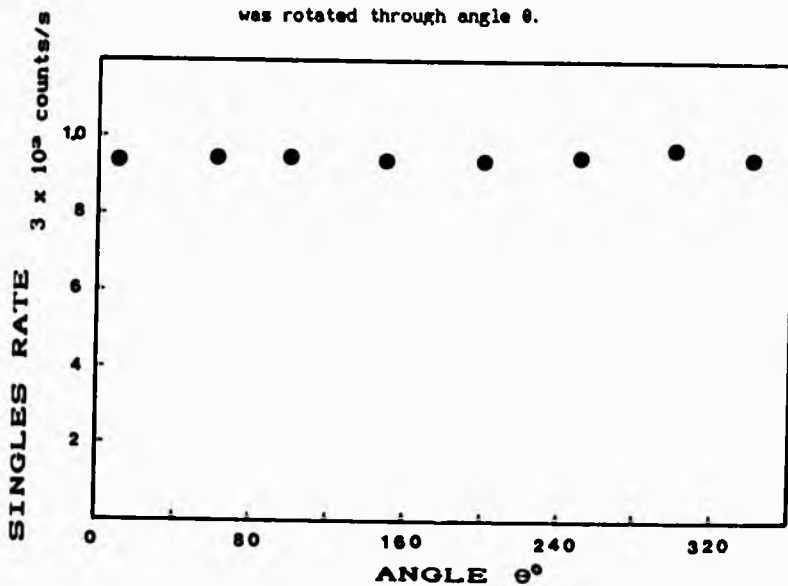


Figure 4.4. A plot of the singles rate as the fast axis of the $\lambda/2$ -wave plate was rotated through angle θ .

observation axis, is given in figure 4.4, from which it is clear that no significant variation of the singles rate was found as the fast axis of $\lambda/2$ -wave plate was rotated.

iii) Comparison of the results with the predictions of quantum mechanics and local realism

As discussed in § 1.1, the most appropriate form of Bell's inequality for experimental studies of polarization correlation is the Freedman's form, given by (cf. inequality (1.4))

$$\eta = [R(22.5^\circ) - R(67.5^\circ)]/R(\infty) \leq 0.25 \quad (4.1)$$

Consulting Eq. (2.44), in chapter 2, the quantum mechanical prediction for this experiment is given by

$$\frac{R(\theta)}{R(\infty)} = 0.2199 + 0.1928 \cos 2\theta \quad (4.2)$$

Substituting the measured values of all the parameters in Eq. (4.2) above (cf. § 3.2), one can compute η . Thus

$$\eta_{\text{qm}} = 0.272 \pm 0.008 \quad (4.3)$$

The experimental result on the other hand was found to be

$$\eta_{\text{exp}} = 0.271 \pm 0.021 \quad (4.4)$$

Hence, we can conclude that the experimental result violates inequality (4.1), and is in good agreement with the quantum mechanical prediction. The result,

represented in figure 4.2, is very similar to that reported earlier by Perrie *et al*(27), as shown in figure 4.5, in which the two-photon radiation was analysed by two linear polarizers only, without the $\lambda/2$ -wave plate. They found η_{exp} equal to 0.268 ± 0.010 . Taking a weighted mean of this result with the present result (quantum mechanically justifiable, since the insertion of the $\lambda/2$ -wave plate does not effect the measured coincidence signal (cf. Eq.(2.47)) we find the value $\eta_{exp} = 0.269 \pm 0.009$ violating Bell's inequality by more than two standard deviations.

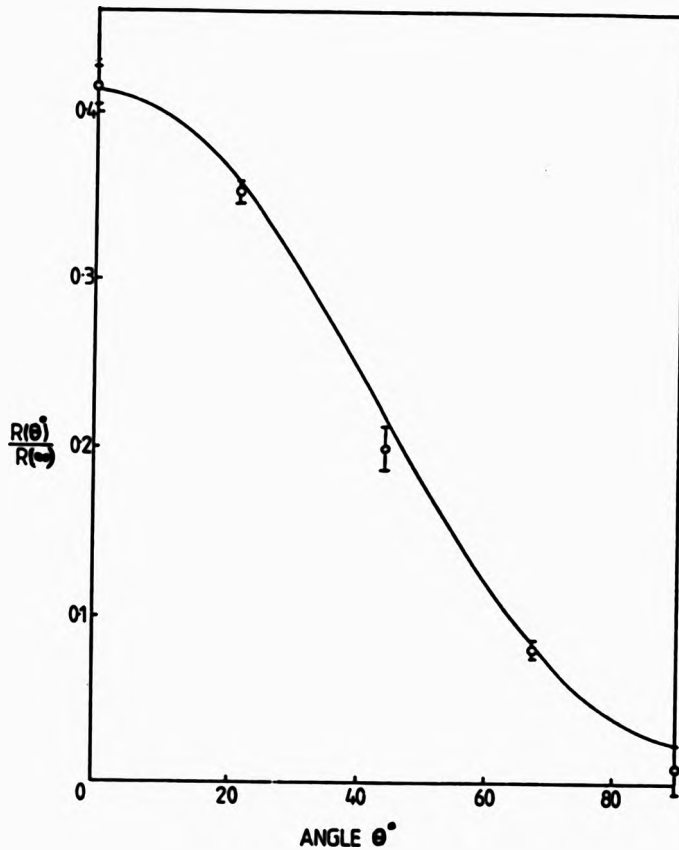


Figure 4.5. Coincidence signal as a function of the angle θ between the transmission axes of the polarizers, relative to $R(\infty)$, the coincidence signal with the polarizer plates removed. The solid curve represents the quantum mechanical prediction (Perric et al. 1971).

§ 4.2 THREE LINEAR POLARIZERS.

In a further experiment, to test local realistic models of a type originally suggested by Garuccio and Selleri(30), which included the possibility of enhanced photon detection, three linear polarizers were used. Their model is consistent with single photon physics and all measurements of two-photon polarization correlations so far described. However, the model predicts a discrepancy with quantum mechanics in the case of the three polarizer experiment.

1) Measurements.

Figure 4.6 displays the detection system used in this experiment. In addition to the two linear polarizers, A and B, another linear polarizer (polarizer C) was

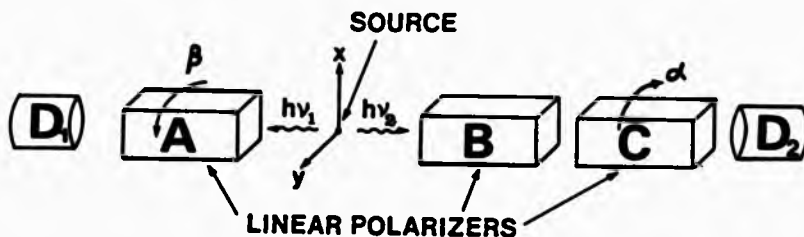


Figure 4.6. Schematic diagram of the three polarizer experiment.

inserted in between polarizer B and the adjacent photomultiplier. The orientation of polarizer B was held constant while polarizer A was rotated through an angle β in the direction shown in the figure and polarizer C through an angle α in the opposite sense. The quantity $R(\beta, \alpha)/R(\beta, \infty)$ was then measured for various angles β as a function of the angle α , where, as defined in § 2.3, $R(\beta, \alpha)$ is the two-photon coincidence rate with all polarizer plates in place while $R(\beta, \infty)$ is the rate with the plates of polarizer C removed.

11) Results

The experimental results for $\beta = 0^\circ$, 33° and 67.5° are shown in figures 4.7 and 4.8 along with the quantum mechanical predictions as solid lines. Also shown, as a dotted line in figure 4.7, is the upper limit for various angles β , set by theories of the Garuccio-Selleri type, for the ratio $R(\beta, \alpha)/R(\beta, \infty)$.

Figure 4.9 demonstrates the coincidence rates at $\alpha = 45^\circ$ and -45° for $\beta = 67.5^\circ$. This result allows us, assuming the validity of the quantum mechanical formalism, to determine the effective value of $\Delta(\beta, \alpha)$, measured by using the two-photon signal, since we have,

$$[R(67.5^\circ, -45^\circ) - R(67.5^\circ, 45^\circ)]/R(67.5^\circ, \infty) = 2\Delta(67.5^\circ, |45^\circ|)$$

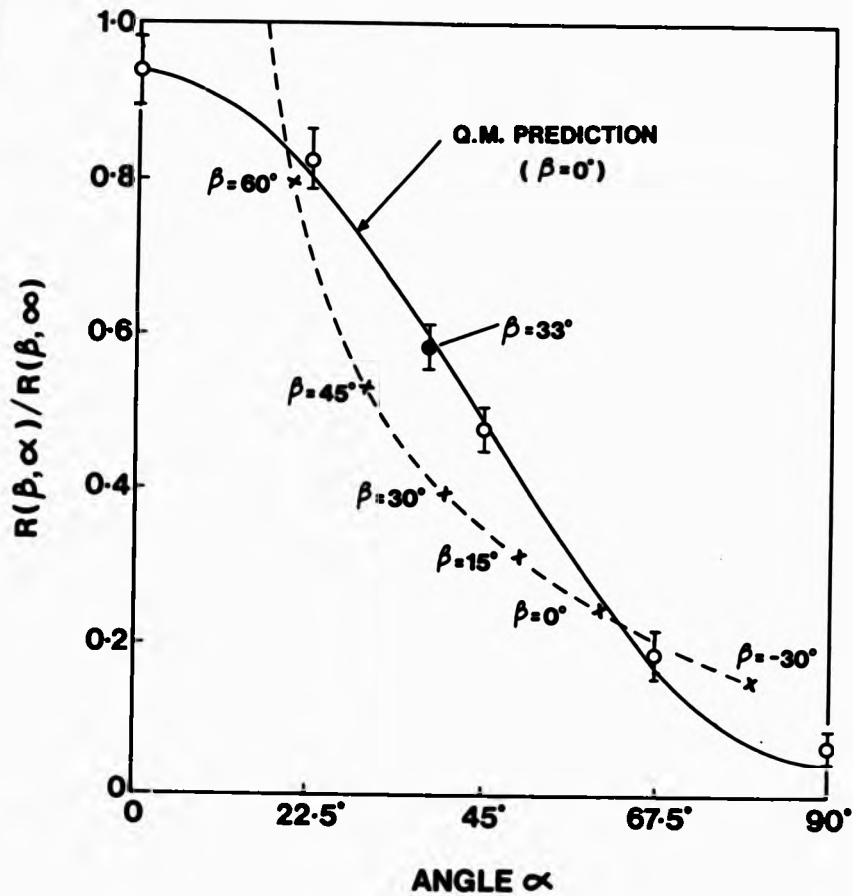


Figure 4.7. Variation of the ratio $R(\beta, \alpha)/R(\beta, \infty)$, for $\beta = 0^\circ$ and 33° , as a function of α . The quantum mechanical prediction for $\beta = 0^\circ$ is shown as the solid curve whereas the upper limit for various angles β set by theories of the Garuccio-Salleri type is shown as a dotted line.

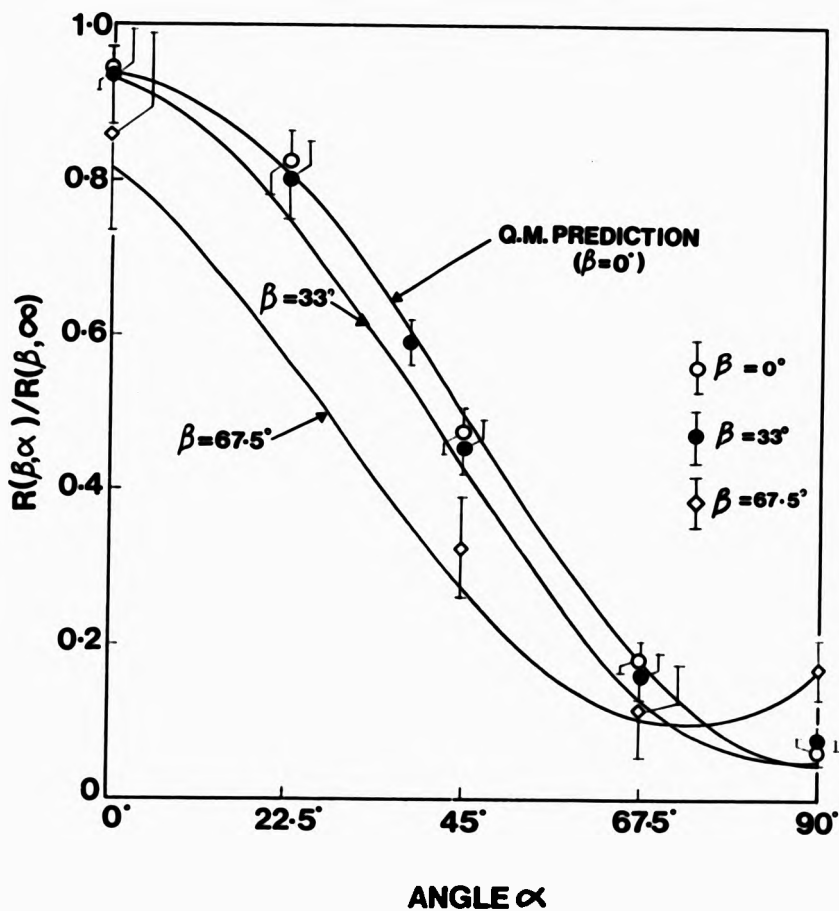


Figure 4.8. Variation of the ratio $R(\beta, \alpha)/R(\beta, \infty)$ as a function of α , for $\beta = 0^\circ, 33^\circ$ and 67.5° . The solid curves represent the quantum mechanical predictions.

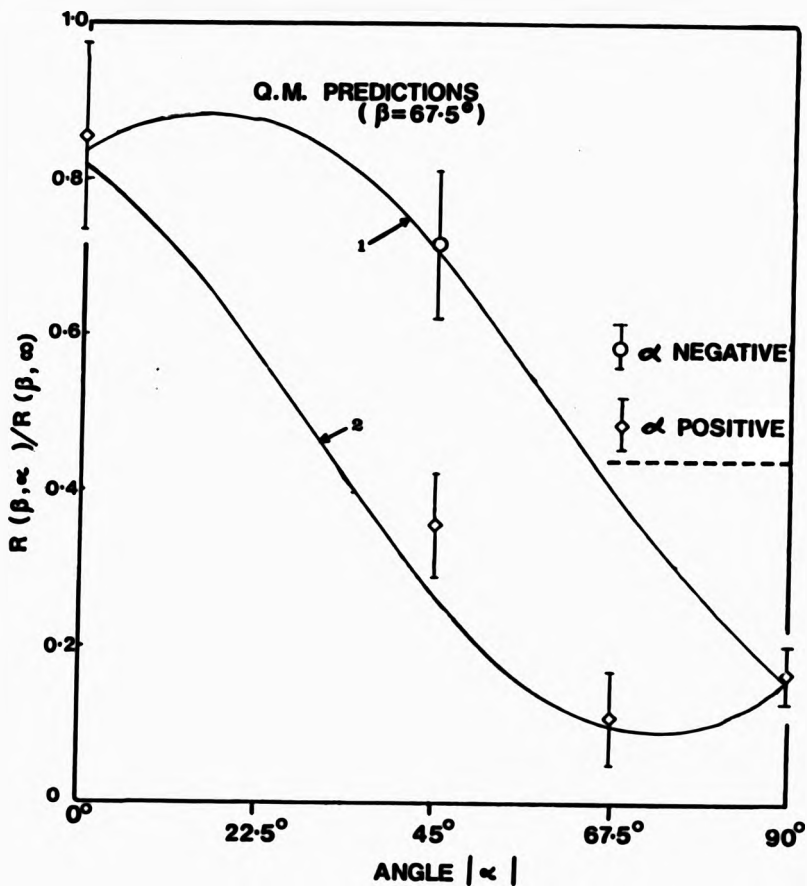


Figure 4.9. Variation of the ratio $R(\beta, \alpha) / R(\beta, \infty)$ as a function of α , for $\beta = 67.5^\circ$. The solid curves represent the quantum mechanical predictions for (1) - α and (2) α .

Substituting the measured values of the parameters (cf. Table 3.1) in Eq. (2.55), and taking into consideration the incoherency dependence of the multiply reflected beam on the wavelength (since the contribution of the beam resulting from internal reflections in the polarizers depends on the variation of the reflectivity of the Suprasil plates with wavelength and the variation of the absorption of the plates with wavelength which, in the case of the achromatic two-photon beam, necessitates averaging over the entire spectral distribution), we can write[49]

$$\frac{R(67.5^\circ, \alpha)}{R(67.5^\circ, \omega)} = 0.4873 + 0.3325\cos 2\alpha - 0.2074\sin 2\alpha \quad (4.5)$$

From the above equation, quantum mechanics predicts $\Delta(67.5^\circ, 145^\circ 1)_{qm} = 0.2074$, which is in agreement with the experimental result (see figure 4.9), $\Delta(67.5^\circ, 145^\circ 1)_{exp} = 0.1805 \pm 0.0570$. These results are also in agreement with that obtained using a monochromatic light source (Hg 254 nm line), as shown in figure 3.6, where $\Delta(67.5^\circ, 145^\circ 1)_{Hg} = 0.1975 \pm 0.0525$ (cf. § 3.2).

iii) Comparison of the results with the predictions of quantum mechanics and local realism

The measurements for $\beta = 0^\circ$, although in excellent agreement with quantum mechanics, which predicts that (cf. Eq. (2.55))

$$\frac{R(0^\circ, \alpha)}{R(0^\circ, \theta)} = 0.4873 + 0.4495\cos 2\alpha, \quad (4.6)$$

as can be seen by reference to figure 4.7, do not suffice to provide a conclusive test between quantum mechanics and the Garuccio-Selleri approach. This result, however, can be regarded as a test of Malus' law for the transmission of polarized light from a very weak source through polarizer C. However, the result for $\beta = 33^\circ$ and $\alpha = 38^\circ$ violates the upper limit of the Garuccio-Selleri model by more than six standard deviations and provides strong evidence against theories of the kind proposed by them. Similarly to Eq. (4.5), we can write the quantum mechanical prediction for the experiment with $\beta = 33^\circ$ in the form [49]

$$\frac{R(33^\circ, \alpha)}{R(33^\circ, \theta)} = 0.4873 + 0.4382\cos 2\alpha - 0.0738\sin 2\alpha. \quad (4.7)$$

The predictions of quantum mechanics, represented in Eqs. (4.5) - (4.7), are plotted as the solid lines in figures 4.7 - 4.9, from which, we can conclude that the experimental results are in overall satisfactory agreement with the predictions of quantum mechanics.

§ 4.3 CIRCULAR POLARIZERS.

1) Measurements.

The measurements of the circular polarization correlation of the two-photon pair utilized achromatic $\lambda/4$ -wave plates and pile-of-plates linear polarizers. The achromatic $\lambda/4$ -wave plates were inserted in each detection arm of the apparatus between the collimating lens and the linear polarizer as shown in figure 4.10. The transmission axes of polarizers A and B were aligned with the y and x axes, respectively and were, thus, perpendicular to each other. Polarizer A and the $\lambda/4$ -wave plate 1 were arranged to form an analyser for light of right handed helicity. Hence, the fast axis of the $\lambda/4$ -wave plate 1 was orientated at 45° to the transmission

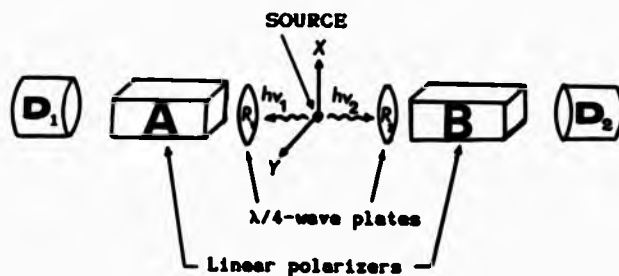


Figure 4.10. Schematic diagram of the circular polarizer experiment.

axis of polarizer A. In the other arm, the fast axis of $\lambda/4$ -wave plate 2 was then rotated from a position where that arm acted as an analyser of light of left handed helicity (the fast axes of $\lambda/4$ -wave plates 1 and 2 were perpendicular) to a position where it acted as an analyser of light of right handed helicity (the fast axes of $\lambda/4$ -wave plates 1 and 2 were parallel).

11) Results

The outcome of the measurements is shown in figure 4.11, along with the quantum mechanical predictions for the circular polarizers used in this experiment. We found that the coincidence rate in this case is lower than that of the linear polarization results. This reduction in rate is due to reflection losses (the transmission of the $\lambda/4$ -wave plates is 0.7), coupled with the small diameter of the plates which reduces the collection solid angle considerably. In addition, the light rays from the source, after collimation, could be at an angle of $\pm 2^\circ$ to the detection axis and thereby can cause the retardation of the $\lambda/4$ -wave plates to vary from the ideal by as much as $\pm 15\%$ (instead of $\pm 10\%$ for a ray incident at $\pm 1^\circ$ to the normal).

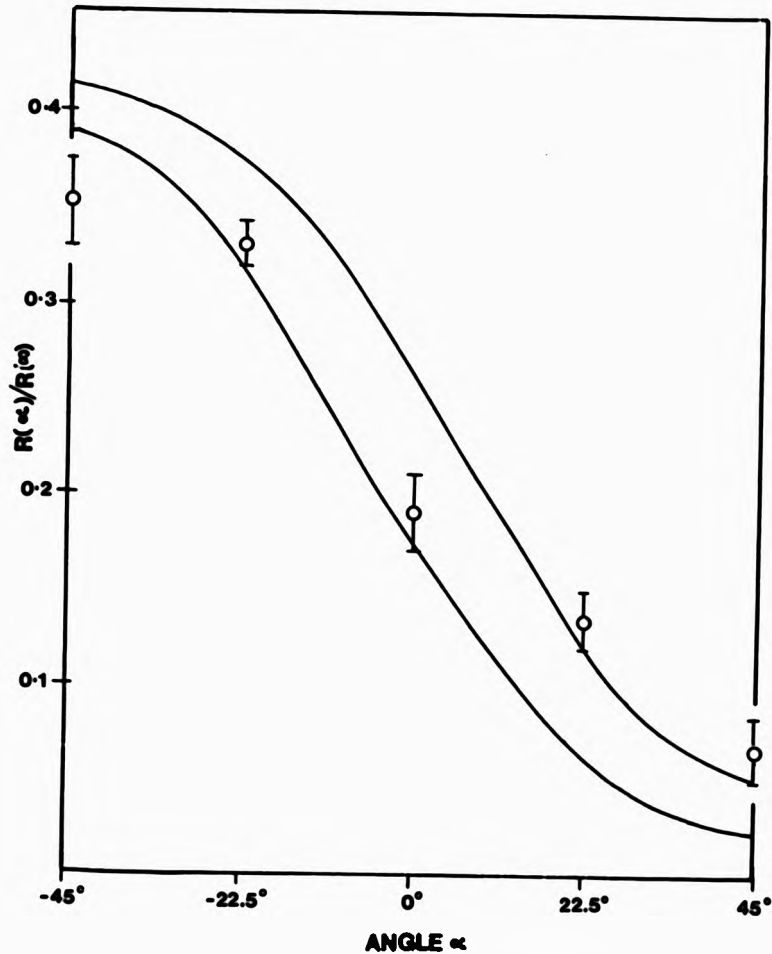


Figure 4.11. Coincidence signal $R(\alpha)$ (α is the angle between the fast axis of the $\lambda/4$ -wave plate and the x-axis) relative to $R(0)$ (the coincidence signal with the polarizer plates removed). The solid curves represent the quantum mechanical predictions.

iii) Comparison of the results with the predictions of quantum mechanics and local realism

The prediction of quantum mechanical theory is (cf. Eq. (2.58) and Table 3.1),

$$\begin{aligned} \frac{R(\alpha)}{R(\omega)} = & 0.2199 - 0.1928 \cos \epsilon_1 \\ & - 0.1928 \sin \epsilon_1 \sin \epsilon_2 \sin 2\alpha \\ & + 0.1928 \cos \epsilon_1 (1 - \cos \epsilon_2) (\sin 2\alpha)^2. \end{aligned} \quad (4.8)$$

where the quantities $R(\alpha)$ and $R(\omega)$ are as defined in § 2.3. Experimentally we found

$$\eta_{\text{exp}} = 0.195 \pm 0.016 \quad (4.9)$$

in agreement, within the limits of error, with the quantum mechanical prediction given by Eq. (4.8),

$$\eta_{\text{qm}} = 0.259 \pm 0.064. \quad (4.10)$$

The low value of η_{exp} is most probably due to the imperfection of the analysers, in particular the retardation of the $\lambda/4$ -wave plates, since, in the case where we have $\epsilon_1 = \epsilon_2 = 90^\circ$, quantum mechanics actually predicts that $\eta_{\text{qm}} = 0.274 \pm 0.008$, in violation of Bell's inequality. In an ideal case, of course, $\eta_{\text{qm}} = 0.354$ ($\epsilon_1 = \epsilon_2 = 90^\circ$, $\epsilon_{\text{mA}} = \epsilon_{\text{mB}} = 1$ and $\epsilon_{\text{mA}} = \epsilon_{\text{mB}} = 0$), and it would be expected that the form of the state vector $|\psi\rangle = [|R1\rangle |R2\rangle + |L1\rangle |L2\rangle] / \sqrt{2}$ (cf. Eq. (2.8)) should result in a $1/4[1 - \sin 2\alpha]$ variation in the quantity $R(\alpha)/R(\omega)$, as

predicted by Eq. (4.8). Although they do not violate Bell's inequality, the results of the circular polarization measurements are important since they verify, within the limit of statistical accuracy, the conservation of angular momentum for the photon pair along the common axis of detection (z-axis).

§ 4.4 THE EFFECTS OF AN ELECTRIC FIELD

The polarization correlation of the two-photon radiation was measured in the presence of an electric field applied perpendicularly to the beam motion to study the effects of the electric field on the emission process. No such measurements have ever been carried out before. An electric field strength of 30 Vcm^{-1} was applied at the observation region and the two-photon radiation was analysed by two polarizers, A and B. Measurements were carried out as follows: First, the transmission axis of polarizer A was held fixed along the x-direction (parallel to the electric field vector), then coincidence rates were recorded as the transmission axis of polarizer B was rotated through angles θ with respect to the x-axis, where $\theta = 0^\circ, 22.5^\circ, 45^\circ, 67.5^\circ, 90^\circ$ and -45° . The results are shown in figure 4.12, along with the results obtained in the absence of an electric field[27]. In order to determine the effective Stoke's parameters of the two-photon beam, the circular polarization correlation was then measured. The results are,

$$P_1 = -0.248 \pm 0.204$$

$$P_2 = 0.014 \pm 0.159 \quad \dots\dots\dots (4.11)$$

$$P_3 = 1.101 \pm 0.337$$

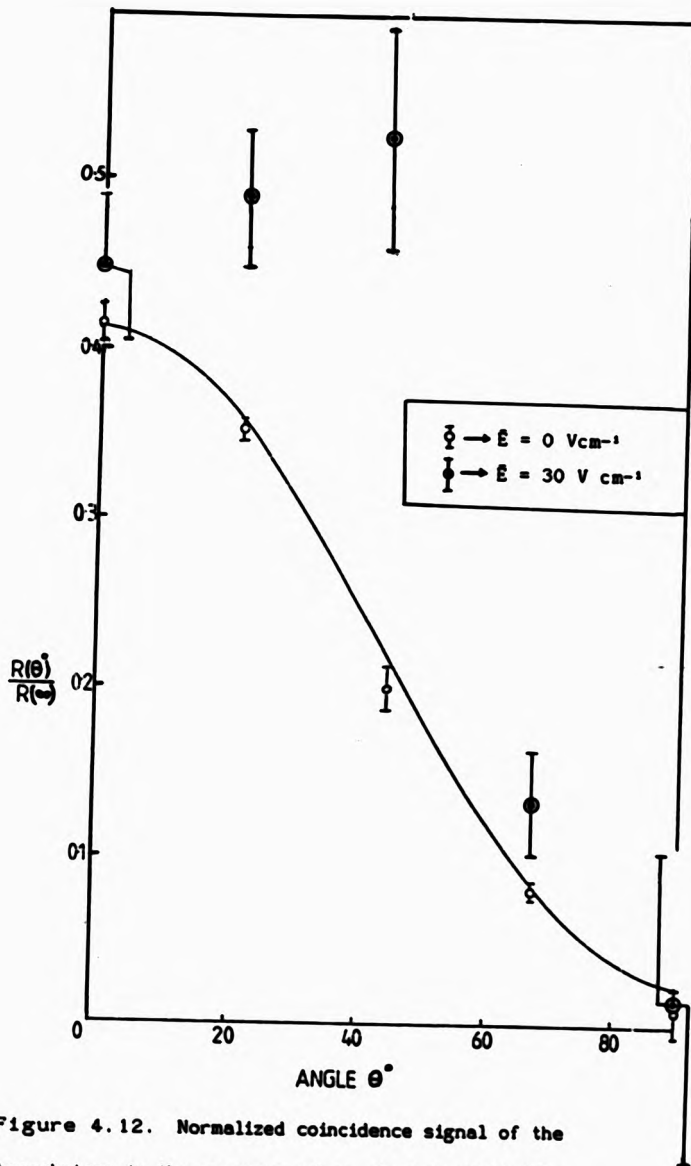


Figure 4.12. Normalized coincidence signal of the two-photons in the presence of an electric field ($E = 30 \text{ V cm}^{-1}$) as a function of θ , the angle between the transmission axis of polarizer B and the electric field vector (x-axis). Quantum mechanical prediction for $E = 0 \text{ V cm}^{-1}$ is shown as a solid curve.

where P_1 , P_2 , and P_3 are defined in the appendix (cf. Eq. (A.28.a) - (A.28.c)). [Note that, if the two-photon radiation is in a pure state, represented by equation (2.10), one would expect $P_1 = 0$, $P_2 = 0$, and $P_3 = 0.94$]. It follows that we can write the effective density matrix as (see the appendix, cf. Eq. (A.27))

$$\rho = \frac{1}{2} \begin{bmatrix} 2.101 \pm 0.337 & -0.248 \pm 0.204 - i[0.014 \pm 0.159] \\ -0.248 \pm 0.204 + i[0.014 \pm 0.159] & -0.101 \pm 0.337 \end{bmatrix} \quad \dots\dots\dots (4.12)$$

Since the Stoke's parameters were measured with a pair of polarizers placed on both sides of the detection arms, the density matrix above does not represent a density matrix describing the polarization state of the two-photon beam but rather an effective density matrix describing the state of polarization of the radiation analysed by polarizer B. Figure 4.12 seems to indicate that the two-photon radiation is polarized at an angle of $\approx 22.5^\circ$ with respect to the x-axis. We can calculate the fraction x of polarized photons in a state of a pure polarization, as defined in the appendix (cf. the appendix, Eq. (A.32)), as the following

$$x = [P_1^2 + P_2^2 + P_3^2]^{1/2} \\ x = 1.129 \pm 0.425 \quad \dots\dots\dots (4.13)$$

The density matrix describing the state of polarization of the two-photons in the case where the electric field $E = 0 \text{ Vcm}^{-1}$ is expected to be

$$\rho = \frac{1}{2} \begin{bmatrix} 1.94 & 0.00 \\ 0.00 & 0.06 \end{bmatrix} \quad \dots\dots\dots (4.14)$$

The fraction of photons in a state of pure polarization, in this case, is $x = 0.97$

In order to determine the state of polarization of the two-photon radiation directly, one has to measure the Stoke's parameters with one polarizer, placed on one side of the detection arms, only. If the determinant of the density matrix obtained is zero, then it implies that the polarization state of the two-photon radiation is a pure state (cf. the appendix, Eqs. (A.22) and (2.27)).

CHAPTER FIVE

CONCLUSION

The vast majority of the various experiments related to the EPR question, reported to date, have confirmed the validity of quantum mechanical theory and violated Bell's inequality, thus appearing to render a local realistic view of the world untenable. However, in all experiments there are severe practical difficulties, particularly because photon detectors are not 100 % efficient and due to this problem, some physicists argue that a decisive test has not been made. These physicists maintain that the photons that are not detected may have different properties from, and are not representative of, those that are detected - the property known as enhancement.

As discussed in § 1.3, a further consideration of these problems was made by, for example, Garuccio and Selleri which led to the derivation of a new form of local realistic model, taking into consideration the possibility of enhanced photon detection[30]. Such a model has been tested by the series of measurements, reported in this thesis, involving measurements of the polarization correlation properties of the two photons emitted simultaneously in the true spontaneous second order radiative decay process in the system of atomic deuterium.

The results of the linear polarization correlation measurements in conjunction with a $\lambda/2$ -wave plate violate Bell's inequality and verify the CHSH form of the no-

enhancement hypothesis. In other words it has been shown that, insofar as it is acceptable to think in terms of individual photons emerging from the polarizers, the probability of the joint detection of the two photons is independent of the relative angle between their planes of linear polarization just prior to detection. In another experiment, where three linear polarizers were employed, the results specifically rule out local realistic models of the type proposed by Garuccio and Selleri in which the probability of a joint detection is dependent on the angle between the detection vector $\bar{\lambda}$ and the polarization vector \bar{i} . In these novel, hitherto unexplored situations the results, do in fact, verify the theoretical calculations based on the quantum mechanical formalism. Hence, we can conclude that local realistic models attempting to explain the results have once again failed.

Although the results support the assumption that there is no enhancement in the detection process, they do not rule out completely the possibility that, because the detector efficiencies are quite low, there may exist some kind of bias or enhancement arising as a result of the employment of the analysers themselves. In other words, the mere presence of the analysers may influence the properties of the photon pairs, in ways other than that suggested by Garuccio and Selleri and subsequently their probability of joint detection. This possibility, of course, would

not exist if the detectors always registered every photon entering them.

The results of measurements performed on the circular polarization correlation verify the conservation of angular momentum for each photon pair and agree with the prediction of quantum mechanics. However, the circular polarization results did not provide a conclusive test of Bell's inequality which was probably due to the imperfection of the achromatic $\lambda/4$ -wave plates used in the experiment.

Finally, it is interesting and perhaps surprising to note that the polarization properties of the two-photons are affected substantially by electric fields. Even for electric fields of only 30 V cm^{-1} , the observed radiation appears to be polarized, possibly because the electric field removes the degeneracy of the virtual intermediate states. However the precise nature of the effect is uncertain and there is no theoretical prediction to look to for guidance. In this case, the polarization state of the two-photon beam may, in fact, no longer be able to be represented by a pure state vector. In fact the results suggest that, within the limits of experimental error, the two-photon radiation has a component linearly polarized at an angle of about 22.5° with respect to the x-axis.

A more complete investigation of the nature of two-photon radiation should now be attempted with the present apparatus by improving the statistical accuracy of the Stoke's parameters and demonstrating beyond doubt, for instance, the possible existence of anisotropy in the emission of polarized photons with respect to the orientation of an electric or magnetic field. Such a study would, in fact, be at the frontier of research into the emission process of two-photon radiation and pioneer research into the effect of fields on the virtual intermediate states of atoms in spontaneous decay processes in what is an essentially new branch of physics.

REFERENCES

References

1. P. Dirac, Proc. Roy. Soc. A, 123 714 (1929).
 2. B. d'Espagnat, Conceptual Foundations of Quantum Mechanics (Second Edition), Benjamin, Reading, Mass. (1976).
 3. A. Einstein, B. Podolsky and N. Rosen, Phys. Rev. 47 777 (1935).
 4. N. Bohr, Phys. Rev. 48 696 (1935).
 5. J. von Neumann, Mathematische Grundlagen der Quantenmechanik, Springer, Berlin (1932); Mathematical Foundations of Quantum Mechanics, Princeton University Press, Princeton, N. J. (1955).
 6. D. Bohm, Phys. Rev. 85 166 (1952).
 7. D. Bohm, Quantum Theory, Prentice-Hall, Engelwood Cliffs, N. J. (1951).
 8. D. Bohm and Y. Aharonov, Phys. Rev. 108 1070 (1957).
 9. C. S. Wu and I. Shaknov, Phys. Rev. 77 136 (1950).
 10. E. Schrödinger, Proc. Camb. Phil. Soc. 31 555 (1935).
 11. W. H. Furry, Phys. Rev. 49 393 (1936).
 12. J. S. Bell, Physica (N.Y.) 1 195 (1964).
-

References

13. J. S. Bell, Rev. Mod. Phys. 48 447 (1966).
 14. J. F. Clauser and M. A. Horne, Phys. Rev. D10 526 (1974).
 15. J. F. Clauser M. A. Horne, A. Shimony and R. A. Holt, Phys. Rev. Lett. 23 880 (1969).
 16. S. J. Freedman, PhD Thesis, University of California, Berkeley (1972).
 17. S. J. Freedman and J. F. Clauser, Phys. Rev. Lett. 28 938 (1972)
 18. R. A. Holt and F. M. Pipkin, Harvard University preprint (1974).
 19. F. M. Pipkin, in: Advances in Atomic and Molecular Physics (D. R. Bates and B. Bederson, eds.), Vol. 14, pp. 281-340, Academic Press, New York (1987).
 20. J. F. Clauser, Phys. Rev. Lett. 36 1223 (1976).
 21. J. F. Clauser, Nuovo Cimento B 33 740 (1976).
 22. E. S. Fry and R. C. Thomson, Phys. Rev. Lett. 37 465 (1976).
 23. A. Aspect, P. Grangier and G. Roger, Phys. Rev. Lett. 47 460 (1981).
-

References

24. A. Aspect, P. Grangier and G. Roger, Phys. Rev. Lett. 49 91 (1982).
 25. A. Aspect, Phys. Rev. D 14 1944 (1976).
 26. A. Aspect, J. Dalibard and G. Roger, Phys. Rev. Lett. 49 1804 (1982).
 27. W. Perrie, A. J. Duncan, H. J. Beyer and H. Kleinpoppen, Phys. Rev. Lett. 54 1790 (1985) and 54 2647(E) (1985).
 28. T. W. Marshall and E. Santos, Phys. Lett. A, 107 164 (1985).
 29. M. Ferrero and E. Santos, Phys. Lett. A, 116 356 (1986).
 30. A. Garuccio and F. Selleri, Phys. Lett. A, 103 99 (1984).
 31. T. W. Marshall, E. Santos and F. Selleri, Phys. Lett. A, 98 5 (1983).
 32. T. W. Marshall, Phys. Lett. A, 99 163 (1983).
 33. M. Ferrero and E. Santos, Phys. Lett. A, 108 373 (1985).
 34. D. Home and T. W. Marshall, Phys. Lett. A, 113 183 (1985).
-

References

35. F. Selleri, Phys. Lett. A, 108 197 (1985).
 36. D. O'Connell, K. J. Kollath, A. J. Duncan and H. Kleinpoppen, J. Phys. B 8 L214 (1975). See also D. O'Connell, PhD Thesis, Stirling University, (1975).
 37. M. Goepfert-Mayer, Ann. Phys. 9 273 (1931).
 38. G. Breit and E. Teller, Astrophys. J. 91 215 (1940).
 39. L. Spitzer and J. L. Greenstein, Astrophys. J. 114 407 (1951).
 40. J. Shapiro and E. Breit, Phys. Rev. 113 179 (1959).
 41. S. Klarsfeld, Phys. Lett. 30A 382 (1969).
 42. B. A. Zon and L. P. Rapaport, Sov. Phys. JETP 7 52 (1968).
 43. W. R. Johnson, Phys. Rev. Lett. 29 1123 (1972).
 44. S. P. Goldman and G. W. F. Drake, Phys. Rev. A, 24 (1981).
 45. F. A. Perpia and W. R. Johnson, Phys. Rev. A, 26 1142 (1982).
 46. W. Perrie, PhD Thesis, Stirling University, (1985).
-

References

47. M. Bacal and W. Reichelt, *Rev. Sci. Instr.*, **45** 769 (1974).
48. G. Spiess, A. Valance and P. Pradel, *Phys. Rev. A*, **6** 746 (1972).
49. A. J. Duncan, private communication.

APPENDIX
DESCRIPTIONS OF THE
POLARIZATION OF LIGHT

In this appendix, we study the state vector and density matrix description of polarized photons, using both linear and circular polarization basis states, and then discuss the description of polarization by use of the Poincaré vector and Stoke's parameters.

§ A.1 QUANTUM MECHANICAL DESCRIPTION OF PHOTONS

To describe a photon, all we need to know are its vector momentum and polarization state. However, since we are only interested in the state of polarization, we treat all photons throughout this discussion as having a single, well-defined frequency and hence momentum.

A.1.1 State Vector

In the classical theory, polarized light, propagating say in the z-direction, can be described in terms of an electric field which oscillates in the x-direction, called x-polarized light, or an electric field which oscillates in the y-direction, called y-polarized light. For a *single* photon there is no electric field that can be discussed in the same way. However, a photon has to have some property which is analogous to the classical phenomenon of polarization. In the case of a photon beam in a *pure state* of polarization, it is possible to describe *all* and *each* of the photons by assigning to the beam or each photon a *single* state vector $|\theta\rangle$ which can be written as a linear superposition of two mutually

orthogonal basis states $|x\rangle$, classically x-polarized light, and $|y\rangle$, classically y-polarized light. Thus we have

$$|\theta\rangle = |a_1|e^{i\phi_1}|x\rangle + |a_2|e^{i\phi_2}|y\rangle \quad (\text{A.1.a})$$

or equivalently,

$$|\theta\rangle e^{-i\phi_1} = |a_1||x\rangle + |a_2|e^{i\delta}|y\rangle \quad (\text{A.1.b})$$

where ϕ_1 and ϕ_2 are the phases, $\delta = \phi_2 - \phi_1$, and a_1 and a_2 are complex numbers. In order to construct such a linear superposition, it is necessary that there is a definite phase relation between the two components. The state vector $|\theta\rangle$ has four real parameters to be determined. However, for unnormalized $|\theta\rangle$, measurement allows us to find only two parameters, the quantity $|a_1|^2/|a_2|^2$ which gives the relative probability of finding the photons in an x-polarized or y-polarized state respectively and the relative phase δ . However, since in the case where the state $|\theta\rangle$ is normalized,

$$|a_1|^2 + |a_2|^2 = 1 \quad (\text{A.2})$$

it follows that the only remaining unknown is the common phase factor of the components of $|\theta\rangle$, but this is unimportant since $|\theta\rangle$ and $|\theta\rangle e^{-i\phi_1}$ represent the same state. The state vector $|\theta\rangle$ can also be represented by a two-dimensional column vector:

$$|0\rangle = \begin{bmatrix} |a_1| \\ |a_2|e^{i\delta} \end{bmatrix}$$

and its adjoint by a row vector:

$$\langle 0| = (|a_1|, \quad |a_2|e^{-i\delta}, \quad \dots \dots \dots) \quad (\text{A. 3})$$

The phase difference has the value:

$$\delta = m\pi \quad (\text{A. 4})$$

for linearly polarized photons, where $m = 0, 1, 2, \dots$,
and for circularly polarized photons:

$$\delta = n\pi/2 \quad (\text{A. 5})$$

where $n = 1, 3, 5, \dots$

Therefore, we may write a state vector $|\chi\rangle$ which describes linearly polarized photons as the following (cf. Eqs. (A. 3) and (A. 4))

$$|\chi\rangle = \begin{bmatrix} |a_1| \\ \pm |a_2| \end{bmatrix} = |a_1| \begin{bmatrix} 1 \\ 0 \end{bmatrix} \pm |a_2| \begin{bmatrix} 0 \\ 1 \end{bmatrix}$$

The adjoint state is

$$\langle \chi| = |a_1| \langle 1, 0 | \pm |a_2| \langle 0, 1 | \quad \dots \dots \dots (\text{A. 6})$$

For a state $|\chi\rangle$, normalized such that $\langle \chi|\chi\rangle = 1$ then the

angle of polarization is $\tan^{-1} \left\{ \pm \frac{|a_1|}{|a_2|} \right\}$.

For $\delta = \pi/2$ then we can write a state vector $|\xi\rangle$ in the form (cf. Eq. (A.3))

$$|\xi\rangle = \begin{bmatrix} |a_1| \\ \pm i|a_2| \end{bmatrix} \quad \text{and} \quad \langle\xi| = (|a_1|, \mp i|a_2|) \quad (\text{A.7})$$

where $|a_1| = |a_2|$ for circularly polarized photons and $|a_1| \neq |a_2|$ for elliptically polarized photons.

A.1.2 Photon State Vector in Linear and Circular Polarization Bases

The state vector and its adjoint state which describe a whole beam of x-polarized photons are given, in matrix representation, by

$$|x\rangle = \begin{bmatrix} 1 \\ 0 \end{bmatrix} \quad \text{and} \quad \langle x| = (1, \quad 0) \quad (\text{A.8})$$

i. e. $|a_2|$ in Eq. (A.6) is zero. Similarly, for y-polarized photons,

$$|y\rangle = \begin{bmatrix} 0 \\ 1 \end{bmatrix} \quad \text{and} \quad \langle y| = (0, \quad 1) \quad (\text{A.9})$$

To describe circularly polarized photons, we may write (cf. Eq. (A.7))

$$|R\rangle = \frac{1}{\sqrt{2}} \begin{bmatrix} 1 \\ 1 \end{bmatrix}, \quad \langle R| = 1/\sqrt{2} \langle 1, -1 \rangle \quad (\text{A. 10})$$

and

$$|L\rangle = \frac{1}{\sqrt{2}} \begin{bmatrix} 1 \\ -1 \end{bmatrix}, \quad \langle L| = 1/\sqrt{2} \langle 1, 1 \rangle \quad (\text{A. 11})$$

for right-hand circularly polarized photons (negative helicity) and left-hand circularly polarized photons (positive helicity), respectively. The constant $1/\sqrt{2}$ is the normalization factor.

A. 1. 3 Density Matrix

The density matrix was introduced by J. von Neumann in 1927 to describe statistical concepts of quantum mechanics. The polarization density matrix of photons ρ is a tensor of rank two, given by the direct product, designated by \otimes , of the state vector with its adjoint:

$$\rho = |0\rangle\langle 0| \quad (\text{A. 12})$$

It can be constructed in matrix form by applying the rules of direct product matrix multiplication. After evaluation (cf. Eqs. (A. 8) - (A. 9) and (A. 12)), one obtains the following density matrices which describe x-polarized and y-polarized photons, respectively,

$$|x\rangle\langle x| = \begin{bmatrix} 1 & 0 \\ 0 & 0 \end{bmatrix} \quad \text{and} \quad |y\rangle\langle y| = \begin{bmatrix} 0 & 0 \\ 0 & 1 \end{bmatrix}$$

..... (A. 13)

Proceeding along similar lines, we find that the density matrices describing circularly polarized photons take the following forms (cf. Eqs. (A. 10) - (A. 12))

$$|R\rangle\langle R| = \frac{1}{2} \begin{bmatrix} 1 & -1 \\ 1 & 1 \end{bmatrix} \quad \text{and} \quad |L\rangle\langle L| = \frac{1}{2} \begin{bmatrix} 1 & 1 \\ -1 & 1 \end{bmatrix}$$

..... (A. 14)

for right circularly polarized photons and left circularly polarized photons, respectively.

A general density matrix which describes pure polarized photons, is as follows

$$\rho = |\theta\rangle\langle\theta| = \begin{bmatrix} a_1 \\ a_2 \end{bmatrix} \otimes (a_1^* \quad a_2^*)$$

..... (A. 15)

where the asterisk denotes the complex conjugate.

Multiplying out we obtain ρ in the Hermitian form:

$$\rho = \begin{bmatrix} |a_1|^2 & a_1 a_2^* \\ a_1^* a_2 & |a_2|^2 \end{bmatrix} = \begin{bmatrix} \rho_{11} & \rho_{12} \\ \rho_{21} & \rho_{22} \end{bmatrix}$$

..... (A. 16)

which contains all the significant information concerning the polarization state of the photon beam, and describes

the preparations which have been performed on the beam. Unlike $|\theta\rangle$ in Eq. (A.1.A), the phase φ , cancels out in the above derivation. The diagonal elements of the matrix ρ are real and they represent the intensities of the components in x and y directions, however, the off-diagonal elements are generally complex. Thus, the intensity I of the photon beam is the sum of the diagonal elements, the trace (Tr) of the density matrix:

$$\text{Tr}(\rho) = I = \rho_{11} + \rho_{22} \quad (\text{A.17})$$

It follows that for a normalized ρ , the condition:

$$\text{Tr}(\rho) = 1 \quad (\text{A.18})$$

must hold. Experimentally, only a linear polarizer is needed to determine ρ_{11} , ρ_{22} and the real parts of ρ_{12} and ρ_{21} . To determine the imaginary parts of ρ_{12} and ρ_{21} , it is necessary to make a measurement of circular polarization, for which a retarder that introduces a phase shift of a quarter period is also needed (i.e. a $\lambda/4$ -wave plate), in addition to a linear polarizer.

In terms of linear polarization basis states, the density matrix takes the form

$$\rho = [a_1|x\rangle + a_2|y\rangle][a_1^* \langle x| + a_2^* \langle y|]$$

Carrying out the multiplication one obtains

$$\rho = |a_1|^2 |x\rangle\langle x| + |a_2|^2 |y\rangle\langle y| + a_1 a_2^* |x\rangle\langle y| + a_1^* a_2 |y\rangle\langle x| \dots\dots\dots (A. 19)$$

and after substitution then we find (cf. Eqs. (A. 8) and (A. 9)),

$$\rho = |a_1|^2 \begin{bmatrix} 1 & 0 \\ 0 & 0 \end{bmatrix} + |a_2|^2 \begin{bmatrix} 0 & 0 \\ 0 & 1 \end{bmatrix} + a_1 a_2^* \begin{bmatrix} 0 & 1 \\ 0 & 0 \end{bmatrix} + a_1^* a_2 \begin{bmatrix} 0 & 0 \\ 1 & 0 \end{bmatrix} \dots\dots\dots (A. 20)$$

Analogously, in terms of circular polarization basis states, we can deduce the following result (cf. Eqs. (A. 10) and (A. 11))

$$\rho = \frac{1}{2} [a_1 |R\rangle + a_2 |L\rangle] [a_1^* \langle R| + a_2^* \langle L|] = \frac{|a_1|^2}{2} \begin{bmatrix} 1 & -1 \\ 1 & 1 \end{bmatrix} + \frac{|a_2|^2}{2} \begin{bmatrix} 1 & 1 \\ -1 & 1 \end{bmatrix} + \frac{a_1 a_2^*}{2} \begin{bmatrix} 1 & 1 \\ 1 & -1 \end{bmatrix} + \frac{a_1^* a_2}{2} \begin{bmatrix} 1 & -1 \\ -1 & -1 \end{bmatrix} \dots\dots\dots (A. 21)$$

It can be easily shown that ρ is *idempotent*, namely;

$$\rho^2 = \rho$$

and the determinant $|\rho| = 0$.

..... (A.22)

However, the relation (A.22) above is not valid for a more general case where we have a *statistical mixture* of states. Mixtures are incoherent superpositions of the corresponding pure polarization states and can be described *only* by a density matrix, *not* a state vector. It is *not* possible, for a beam of photons in a mixture of states, to transmit *completely* through a linear polarizer. In this case, ρ is no longer idempotent and is given by

$$\rho = \sum_i x_i \rho_i \quad (\text{A.23})$$

where $\rho_i^2 = \rho_i$ (i.e. each ρ_i is a pure state), $x_i \geq 0$ is the weight or the fraction of the intensity of the pure state characterized by ρ_i , and $\sum_i x_i = 1$. In the case of a completely *unpolarized* photon beam, all directions of polarization are equally probable and we may write ρ as

$$\rho = \frac{1}{2} |x\rangle\langle x| + \frac{1}{2} |y\rangle\langle y|$$

* E. Merzbacher, Quantum Mechanics, John Wiley & Sons, Inc. (1967).

$$= \frac{1}{2} \begin{bmatrix} 1 & 0 \\ 0 & 0 \end{bmatrix} + \frac{1}{2} \begin{bmatrix} 0 & 0 \\ 0 & 1 \end{bmatrix}$$

or in the form

$$\rho = \frac{1}{2} |R\rangle\langle R| + \frac{1}{2} |L\rangle\langle L|$$

$$= \frac{1}{4} \begin{bmatrix} 1 & -1 \\ 1 & 1 \end{bmatrix} + \frac{1}{4} \begin{bmatrix} 1 & 1 \\ -1 & 1 \end{bmatrix}$$

..... (A. 24)

There is no fixed phase relationship between the two components of the beam, and from Eq. (A. 24) above it can be easily verified that $\rho^2 \neq \rho$.

§ A.2 CLASSICAL DESCRIPTION OF THE POLARIZATION OF LIGHT

There are two main methods to describe the state of polarization of light - The Poincaré vector and the Stokes parameters method. Each of these methods is useful in allowing the polarization state of a beam to be described in terms of experimental measurements. In dealing with problems involving polarized light, the Poincaré sphere construction is better for giving a qualitative understanding of the problems. In this method, the poles of the Poincaré sphere represent right and left circular polarization, the equator represents linear polarization, and other points on the sphere (above or below the equatorial plane) represent elliptically polarized light. As for quantitative calculations, the Stokes parameters provide a more useful description. We can express ρ in terms of the vector representation of polarized light. Like any arbitrary 2×2 matrix, the density matrix ρ may be written as a linear combination of four independent two-rowed matrices:

$$\rho = \frac{1}{2} (I + \hat{P}(P_1, P_2, P_3) \cdot \hat{\sigma}) \quad (\text{A. 25})$$

where P_1 , P_2 and P_3 are the components of the Poincaré vector \hat{P} , $\hat{\sigma}$ is the vector whose components are the Pauli matrices,

$$\sigma_1 = \begin{bmatrix} 0 & 1 \\ 1 & 0 \end{bmatrix}, \quad \sigma_2 = \begin{bmatrix} 0 & -i \\ i & 0 \end{bmatrix} \quad \text{and} \quad \sigma_3 = \begin{bmatrix} 1 & 0 \\ 0 & -1 \end{bmatrix}$$

..... (A. 26)

and I is a unit matrix. Hence Eq. (A. 25) can be rewritten in the form

$$\rho = \frac{1}{2} \begin{bmatrix} 1 + P_3 & P_1 - iP_2 \\ P_1 + iP_2 & 1 - P_3 \end{bmatrix} \quad (\text{A. 27})$$

In order to specify the density matrix of any given beam, one has to know all the components of the Poincaré vector which are in fact the three real *Stokes parameters*. These are simply the three cartesian coordinates of a point on the Poincaré sphere. In this case, the radius of the Poincaré sphere, corresponding to the intensity of the beam is equal to unity (cf. Eq. (A. 2)). P_1 and P_2 are at right angles to each other in the equatorial plane, and P_3 points toward the north pole of the sphere. These parameters take values between -1 and $+1$ and can be determined through intensity measurements only. For example, it can easily be seen from Eq. (A. 27) that P_3 describes the degree of circular polarization and is given by

$$P_3 = \frac{I(\text{Right}) - I(\text{Left})}{I(\text{Right}) + I(\text{Left})} \quad (\text{A. 28. a})$$

where $I(\text{Right})$ represents the intensity of right-hand polarized light etc. Since right-hand and left-hand

circular polarizations correspond to helicities of the photons, it is clear that P_2 is the mean value of the helicity of the photons. P_3 and P_1 are the degree of linear polarization, given with respect to the x-axis, by, respectively

$$P_3 = \frac{I(0^\circ) - I(90^\circ)}{I(0^\circ) + I(90^\circ)} \quad (\text{A. 28. A})$$

and

$$P_1 = \frac{I(45^\circ) - I(135^\circ)}{I(45^\circ) + I(135^\circ)} \quad (\text{A. 28. c})$$

Circular polarization implies $P_1 = P_3 = 0$ and that, $P_2 = 1$ and -1 for right-hand and left-hand circular polarization, respectively. Linear polarization in the x-direction implies $P_1 = P_2 = 0$ and $P_3 > 0$ (in the y-direction; $P_1 = P_2 = 0$ and $P_3 < 0$). The values of $P_3 = +1$ and -1 therefore correspond to complete polarization in the x and y directions, respectively. The probabilities that the light is linearly polarized along the directions 45° and 135° to the x-axis are, respectively, $\frac{1}{2}(1+P_1)$ and $\frac{1}{2}(1-P_1)$ and the probabilities that the photon has right-hand and left-hand circular polarization are respectively, $\frac{1}{2}(1+P_2)$ and $\frac{1}{2}(1-P_2)$. The magnitude of the Poincaré vector is restricted by

$$|\vec{P}|^2 = P_1^2 + P_2^2 + P_3^2 \leq 1 \quad (\text{A. 29})$$

Generally ρ is a mixture of states. The inequality above becomes an equation if and only if ρ is a pure state. For an unpolarized beam the electric vector changes

rapidly and erratically with time both in its amplitude and its absolute phase, in which case, P_1 , P_2 and P_3 average out to zero. For an elliptically polarized beam the electric vector is also changing rapidly, but in such a way that a_1/a_2 and δ remain constant. In this case P_1 , P_2 and P_3 will have constant values.

For a more general case where a photon beam is partially polarized, one can add an unpolarized term to the pure state polarized density matrix††. Hence (cf. Eq. (A.25))

$$\rho = \frac{1}{2} (x (I + \vec{P} \cdot \vec{\sigma}) + (1 - x) I) \quad (\text{A. 30})$$

where x is the fraction of polarized photons and the last term is the fraction of unpolarized photons. Equation (A.30) can be rewritten in the form:

$$\rho = \frac{1}{2} (I + x \vec{P} \cdot \vec{\sigma}) \quad (\text{A. 31})$$

where, in this case, the Poincaré vector is

$$|\vec{P}|^2 = P_1^2 + P_2^2 + P_3^2 = 1$$

Let us define $\hat{P}_i = x P_i$, where $i = 1, 2, 3$. then, we

$$\text{have } x^2 = \hat{P}_1^2 + \hat{P}_2^2 + \hat{P}_3^2 \leq 1 \quad (\text{A. 32})$$

so that measurement of \hat{P}_1 , \hat{P}_2 and \hat{P}_3 allows x to be found and all properties of the beam to be specified.

†† E. Merzbacher, private communication.